An Experimental Study of the Relative Response of Plastic Scintillators to Photons and Beta Particles within the Context of Tritium Monitoring

By

Ashita Kumar

A Thesis Submitted in Partial Fulfillment

Of the Requirements for the Degree of

Master of Applied Science

In

Nuclear Engineering

Faculty of Energy Systems and Nuclear Science Program

University of Ontario Institute of Technology

August, 2011

Abstract

A scintillation counting system has been constructed with the use of BC-400 and EJ-212 series plastic scintillators along with a subminiature photomultiplier tube to investigate the effect of increasing plastic scintillator thickness on system-integrated counts. Measurements have been carried out using four different gamma sources with different energies ranging from 6keV to 1.332MeV and a Ni-63 beta source of maximum energy of 66keV. A simulation was also carried out in MCNP4a to verify the number of H-3 beta particles with max energy 18.6keV that would reach the plastic scintillator in a vacuum setting as well as in an air medium. Scintillator thicknesses ranged from 10μm to 2500μm. The response of the system was determined by measuring the integrated counts as a function of scintillator thickness. The results of these measurements showed the expected positive linear correlation between scintillator thicknesses and integrated counts for all the gamma sources while the slopes of the correlations of each gamma source was a function of the source energy. The beta particle response showed an initial increase of counts with scintillator thickness followed by a slight decrease. The MCNP simulation confirmed an analytical calculation of the fraction of H-3 beta particles for a given air concentration that would reach the scintillator. These results in conjunction with the experimental findings were used to assess the potential of a plastic scintillator system forming the basis of a tritium monitor for the detection of tritium in high-energy gamma backgrounds for Canadian nuclear power workers.

Keywords: Plastic scintillator, Tritium, MCNP, gamma photons, beta particles

Table of Contents

Abstract 2

Acknowledgments 5

List of Figures 6

List of Tables 8

Nomenclature 9

Acronyms 10

Chapter 1 11

Introduction 11

1.1 Thesis Objectives 14

1.2 Past Trials of Tritium/Gamma detection 17

1.3 Outline of Thesis 21

Chapter 2: Background to Theory 24

2.1 Interaction of Gamma Rays with Matter 24

2.2 Interaction of Beta Particles with Matter 30

2.3 Scintillation Detection 31

Chapter 3: Experimental Set Up 34

3.1 Materials for Experimental Setup 34

3.1.1 Photomultiplier Tube and Plastic Scintillators 34

3.1.2 Testing Chamber 38

3.1.3 Accounting for Uncertainty: 41

3.2 Simulation for MCNP 43

Chapter 4: Results/Discussion of Experimental Work 46

4.1 Gamma Sources 46

4.1.1 Overall Results of Gamma Sources 47

4.1.2 Cs-137 Measurement Difficulties 49

4.1.3 Iron-55 Results 53

4.2 Nickel-63 Beta Source 54

4.2.1 Co-60 Trials with EJ-212 Series Plastic Scintillators 61

4.3 Spectrum Analysis 63

4.4 Optimizing Scintillator Thickness....67
4.5 H-3 Simulation Analysis Results....73
4.5.1 Calculated Hypothesis for H-3 Simulation....73
4.5.2 Simulated Results for the Range of Beta Particles Emitted from Tritium....75
Chapter 5: Future Developments and Related Studies....81
5.1 Stack Monitors....81
5.2 Analysis of Other Investigations....83
Chapter 6: Conclusion....86
Appendix A: MCNP Code for Tritium Simulations....90
Appendix B: Exposure Rate of Co-60 Gamma Source....92
References....97

Acknowledgments

First, I would like to thank Dr. Anthony Waker for the numerous opportunities he has given me throughout my time here at UOIT. I would also like to acknowledge his guidance, supervision and most of all his patience that helped me persevere through the challenges and obstacles faced during the course of this degree.

I would also like to express my deepest gratitude to all my professors at UOIT who have taught me for the past 5 years. Their trust, support, and advice have been of utmost help to the completion of my Undergrad degree as well as my Masters Degree. I am especially grateful to Dr. Rachid Machrafi for helping me understand the importance of radiation fundamentals and basic nuclear engineering concepts during my undergraduate Degree.

I would also like to thank all my colleagues and friends who have given me any design suggestions and for their continued and generous support throughout my time at UOIT.

I am grateful to the University Network of Excellence in Nuclear Engineering (UNENE) and the Natural Sciences and Engineering Council of Canada (NSERC) for their financial contribution to this research.

Lastly, I'd like to dedicate this work to my parents, Marie and Asheesh whose love and support gave me the courage needed to finish this degree and as well to my beloved brother, Gaurav. I would also like to mention my fiancée, Raj, whose support was paramount in making this thesis possible.

List of Figures

Figure 2.1: Visual Description of Compton Scattering 27

Figure 2.2: Visual Description of Pair Production.....…29

Figure 2.3: Plot to differentiate between the occurrences of the three gamma interactions..29

Figure 3.1: The process inside a PMT 35

Figure 3.2: Schematic of a Photo Multiplier Tube 36

Figure 3.3: Schematic of Experimental Setup 37

Figure 3.4: Inside view of electrical box 39

Figure 3.5: PMT and base connections.....40

Figure 3.6: Aluminum holder shown in Google Sketch 40

Figure 3.7: Electrical Box Supported by Wooden Boards Attached by Desk Clamps.....40

Figure 3.8: MCNP Simulation 45

Figure 4.1: Plots of Fe-55 and Am-21 gamma sources versus increasing scintillator thickness.....48

Figure 4.2: Plots of Cs-137 and Co-60 gamma sources versus increasing scintillator thickness.....49

Figure 4.3: Cs-1376 Comparisons to Cut Down Beta Particles.....51

Figure 4.4: Cs-137 Comparisons between 1mm & 0.125 mm Copper Disks.....52

Figure 4.5: Fe-55 Attenuation beyond 500μm Thickness 53

Figure 4.6: Hypothesized results for Ni-63.....56

Figure 4.7: Ni-63 Initial Trials.....57

Figure 4.8: Ni-63 Results shown for integrated counts vs. scintillator thickness.....60

Figure 4.9: Co-60 Results for EJ-212 series plastic scintillators 63

Figure 4.20: VISED setup of MCNP Results... 76

List of Tables

Table 3.1 Uncertainty Regarding Plastic Scintillator Thickness.....38

Table 3.2 Systematical Error for Data Set 1.....42

Table 3.3 Systematical Error for Data Set 2.....42

Table 3.4 Measurement Error of Data Set from Co-60 source.....43

Table 4.1 Attenuation Coefficients of Gamma Sources Used based on Increasing Energy.....46

Table 4.2 Cs-137 Trials to reduce Beta Particle counts…….48

Table 4.3 Result set for gamma photons ……...……....51

Table 4.4 Ni-63 Trials ……...……....60

Table 4.5 Averaged Ni-63 Trials over each thickness and plotted in Figure 5…….....60

Table 4.6 Co-60 Trials.....62

Table 4.7 Averaged Co-60 Trials over each thickness and plotted in Figure 5.....62

Table 4.8 Co-60 and Ni-63 counts comparison.....72

Table 4.9 Constituent Elements of Air.....79

Table 5.1 Table of radionuclides detected by stack monitoring.....82

Table 5.2 Range of Radionuclides used to calculate the volume of air surrounding the detector……...…82

Table 5.3 Stopping Powers for Various beta Sources…….....85

Nomenclature

A	Activity of source (Bq)
Γ	Specific Gamma Ray Constant ($\frac{C \cdot m^2}{kg \cdot MBq \cdot h}$)
Z	Atomic Number
H	Height of cylinder (m)
λ	Decay Constant (sec^{-1})
μ	Attenuation coefficient (cm)
μ_{en}	Energy absorption coefficient (cm^2)
ρ	Density of material ($\frac{g}{cm^3}$)
$T_{1/2}$	Half-Life of a radionuclide (sec)
ϕ	Binding energy ($\frac{MeV}{amu}$)
X_{air}	Exposure rate in air ($\frac{C}{kg \cdot hr}$)
X_1	Distance 1 (m)
X_2	Distance 2 (m)
x	Thickness of medium (cm)
φ	Ionization potential of medium (J)
D	Dose rate ($\frac{Gy}{hr}$)
E	Energy (J)
r	Radius of cylinder (m)
R	Range of Particle ($\frac{mg}{cm^2}$)
W_{air}	Average energy expended in air per ion pair formed ($\frac{J}{C}$)

Acronyms

ALARA	As Low As Reasonably Possible
ALI	Annual Limit Intake
BNC	Bayonet Neill-Concelman Connector
CANDU	Canadian Deuterium Uranium Reactor
COG	CANDU Owners Group
DAC	Derived Air Concentration
DEL	Derived Emission Limit
EJ	Eljen Technologies
ICRP	International Commission on Radiological Protection
ICRU	International Commission on Radiological Units
LLD	Lower-Level Discriminator
MCA	Multi Channel Analyzer
MCNP	Monte Carlo N-Particle
MPCa	Maximum Permissible concentration in air
PMT	Photomultiplier Tube
QE	Quantum Efficiency
SHV	Safe High Voltage connector
ULD	Upper-Level Discriminator
VISED	VISual EDitor

Chapter 1

Introduction

Since the discovery of radiation in 1895 by Wilhelm Rontgen, a German physicist, detectors have played a crucial role in determining the different types of radiation and their effect on the environment and biological matter [1]. Radiation can generally be classified into two (2) main categories; Ionizing radiation and non-ionizing radiation. Non-ionizing radiation possesses insufficient electromagnetic radiation and energy to ionize (remove an electron from) an atom [1]. Microwave radiation is an example of non-ionizing radiation and generally does not pose a threat to human life.

Ionizing radiation however is quite dangerous and has been studied since the discovery of x-rays in 1895. Ionizing radiation can be categorized into four types, which include fast electrons, heavy charged particles, electromagnetic radiation and neutrons. X-rays are produced via two methods one of which includes electrons transition from orbital shells in an atom. The second method is termed bremsstrahlung and occurs when an electron passes close enough to the nucleus which causes it to slow down and deflect from its original path. The loss of kinetic energy from the electron due to this slowing down process is conserved via an x-ray emission. Gamma rays, also included under the category of ionizing radiation and originate from transitions within the nucleus of an atom. It is the decay process of atomic nuclei from higher energy states to lower energy states. Neutrons are characterized by their energy as either fast or slow neutrons while heavy charged particles include energetic ions with a mass equal to or greater than one atomic mass unit. Fast electrons include beta particles emitted during the nuclear decay

processes of radioactive isotopes as well as energetic electrons produced by other processes [3].

Detection of these types of radiation involves building accurate detectors since radiation cannot be detected by human senses.

While ionizing radiation can be a grave hazard, it has proven to be quite useful in medical diagnostics and treatment and even a source of clean energy for electrical power generation. The development of nuclear power has been progressively improving, although suffering setbacks such as the Three Mile Island, Chernobyl and more recently Fukushima. The experiences from these unfortunate events have been valuable and serve to improve nuclear technology each time to create safer, reliable and more efficient plants. Radiation detectors are immensely useful and are an important aspect of research and development in these environments. Detectors monitor nuclear facilities and power plants to ensure proper safety precautions have been implemented to keep workers and the public safe. Monitoring of any and all radioactive releases inside areas of the plant where workers may need to be present is an essential precaution. Others may include containers being improperly closed or secured for transportation.

Depending on the purpose of the detector, they may be constructed in all shapes and sizes but the principal working of all detectors stems from their interaction with different types of radiation. The radiation interacts with a specific material inside the detector and generates a signal then recorded for analysis and interpretation. Many detectors have been developed with a specific purpose, with their own strengths and

weaknesses, some of which can even be calibrated to detect multiple types of radiation in a particular environment.

Detectors may be grouped into gas-filled, solid and liquid state detectors. The gas-filled detectors contain a wire, centralized in a chamber called the "anode" initially carrying a positive voltage with respect to the "cathode", which constitutes the outer walls of the detector. The chamber is filled with a gas that produces ion pairs when interacting with incoming radiation. The electron component of these ion pairs are attracted and collected at the anode, while the positive components of the ion pairs head towards the walls of the chamber. The electrons collected at the anode produce a corresponding signal subsequently detected by the electronics registering as pulse heights. This underlines only the basics of gas-filled detectors. [4, 5]

Solid scintillator detectors incorporate a solid scintillating medium. These radiation types will be covered in the next chapter but briefly put, each of these scintillators produces light due to the interaction of the material with incoming radiation and is converted into an electronic signal output on a rate meter or some other recording device for analytical purposes. Some examples of instruments that contain such media are sodium iodide, zinc sulfide and plastic scintillators. The first two consist of inorganic crystalline solids which produce light flashes with the interaction of certain types of radiation while plastic scintillators are organic detectors that rely on the scintillation process. They are principally used for the detection of beta radiation, while sodium iodide is used for gamma radiation and zinc sulfide is used for alpha radiation [4].

1.1 Thesis Objectives

Tritium is a radioactive isotope of hydrogen. Its nucleus contains 1 proton and 2 neutrons as opposed to hydrogen which contains 1 proton and no neutrons. Tritium can be formed a number of ways including neutron absorption of lithium-6, lithium-7 and boron-10, all of which yield helium-4 and tritium.[1] In nuclear power plants however, tritium is formed by the bombardment of deuterium by neutrons. Tritium decays via beta particles to helium-3^{+}, an isotope of helium-2 having a very large cross-section, that when exposed to thermal neutrons, produces hydrogen and tritium [6]. Cross-section here is defined as the probability of interaction between the incoming particles and the target nucleus. In this case, the nucleus of helium-2 possesses a large probability of interaction when the incoming particle is a thermal neutron. A thermal neutron is classified as one having a kinetic energy of 0.025 eV or lower [1]. A cross-section governs the ability for interactions between any two particles and is a fundamental concept in nuclear physics. Tritium can also be formed via natural pathways such as interactions between cosmic rays and atmospheric atoms. The radioactive decay of tritium emits beta particles with a maximum energy of 18.6 keV and an average energy of 6.2 keV [7]. Radioactive tritium has a half-life of 12.3 years making it an important candidate for detection [7]. The half-life of an isotope determines its life span. It is the time required for exactly half of the isotope to decay. An isotope is generally considered dead after 6 half lives since only 1.5% of the original radioactivity remains. Approximately 74 years would have to pass before the isotope H-3 was considered dead. A high production rate in nuclear power plants drives the presence and consequential monitoring of H-3 at all times. Beta radiation emitted by H-3 can be absorbed by materials such as paper or metal but cannot

penetrate the top dead layer of skin in humans. The main hazard from beta radiation is thus contributed by inhalation or ingestion [6].

Tritium monitoring is especially important in CANDU reactors because of the use of heavy water (deuterium) in the moderators and heat transport systems that produce tritium. Deuterium is another isotope of hydrogen containing 1 neutron, 1 proton and when exposed to a large number of neutrons, undergoes neutron absorption to form H-3 [1]. It is evident then that H-3 will be present in a nuclear power plant, which can potentially contribute as much as 30% toward the occupational hazard of nuclear energy workers [8]. H-3 monitors and detectors are thus indispensible to control H-3 exposure for nuclear energy workers.

The scope of building instruments which handle tritium monitoring have several applications some of which involve personal tritium monitoring, tritium survey meters, portable tritium monitors, fixed tritium monitors, central tritium monitors and even stack effluent monitors. As far as it has been researched, a personal tritium monitor capable of taking direct readings and be comfortably worn by a worker has not yet been developed. Instrumentation for the remaining applications is commercially available depending on the suitability for the many tritium monitoring applications present at CANDU facilities.

The purpose of this research is to develop a personal tritium monitor that is capable of operating in a high energy gamma background. The high energy gamma background simulates the contribution made from high energy sources that are produced in a CANDU power plant such as Cobalt-60, Americium-241 and Cesium-137. The objectives of this research is to analyze the effect of gamma and beta radiation on plastic scintillators using

four different gamma sources which will include iron-55(Fe-55), cobalt-60(Co-60), cesium-137(Cs-137) and americium-241(Am-241), as well nickel-63(Ni-63) as the beta source. Experimental data will be collected on these 5 sources to confirm the effect of gamma and beta radiation on plastic scintillators. As well, a Monte Carlo N- Particle (MCNP) simulation which was created by Los Alamos, will also be conducted to analyze the range of H-3(18.6 keV) beta particles. This data will support the hypothesis for the amount of beta particles emitted by H-3 that may reach the detection material to produce a readout pulse. The experimental data combined with the simulation data will be pooled together to investigate the possibility of building a H-3 monitor capable of operating in a high energy gamma background to be used in nuclear power plants for the safety of nuclear energy workers.

Considerations with the development of such a monitor need to take into account the sensitivity and range. The sensitivity of the monitor would depend on the application. In the case of a monitor built to measure chronic levels, the capability of measuring lower concentrations would be essential as an early warning indicator of exposure over a full working year.

According to ICRP60, recommendations, the yearly dose limit is set at 20 mSv. This means that commitment rates of much less than 10 μSv/h must be reliably detectable and that a dose commitment rate of 10 μSv/h results from exposure to HTO in air at a concentration of $3x10^5$ Bq/m^3 [5].

This value is also considered to be the Derived Air Concentration (DAC) which will be explained in more detail in a later chapter. In radiation protection applications, the

Maximum Permissible Concentrations in air (MPCa) is sometimes a term which is used to refer to a DAC. The term was found confusing and the DAC was recommended to replace MPCa. The DAC will be used later in this investigation to assess the sensitivity of the monitor in a high energy gamma background.

1.2 Past Trials of Tritium/Gamma detection

Understanding past experiments conducted with beta particles and gamma rays on plastic scintillators is essential in developing a good detector as well as understanding the properties governing how these particles interact with matter. Mixed field dosimeter has been a challenge in the past and a personal monitoring device for nuclear energy workers to detect H-3 in high energy gamma backgrounds do not exist.

Research on the topic was done by C.Cowper and R.V Osborne in 1966, where a setup for such a detector was described, but the sensitivity of the system seemed to have been a challenge. This was due to the number of ionizations tritium produces in air. According to the paper, the maximum permissible concentration of tritium in air for occupational exposure at the time was $5x10^{-6}$ μCi/cm^3. This produced as much ionization in air as a gamma-radiation field of 50 μR/hr. This field is about three times the natural background radiation level and is quite low compared to the background present in nuclear power plants. Investigations of tritium in air via plastic scintillators by Cowper and Osborne lead to designs of a portable air monitor. The detector consisted of a double spiral of plastic scintillator enclosed in a cylinder of about 5 cm in diameter and length. The double spiral arrangement permits an air flow path over all the surfaces of the scintillator with an entry and exit port on the side of the enclosing cylinder. Photomultipliers are coupled to the end windows of the cylinder and collect light pulses

which reach the windows by internal reflection from the scintillator surfaces. The photomultipliers operate in coincidence and are connected to a pulse height discriminator. The principal design objective was to minimize the total mass of scintillator since only a surface layer of a few microns thick was required to absorb the tritium beta rays and any additional thickness only caused unwanted gamma sensitivity. Experimental results regarding this design were inconclusive and a published paper was not found [9].

Although personal dosimeters may not exist, general tritium monitoring detectors do exist and are used worldwide.

A paper by M.J. Wood and R. A. Surette [5] which was published in 1994 provides a good summary on past tritium monitoring and detection. The paper states that according to CANDU monitoring requirements and commercial availability, ionization chambers are used primarily as tritium monitoring devices at CANDU sites. Demanding environment conditions require real time measurements in the presence of high energy gamma fields or radioactive gases. This is done via gas-flow proportional counters or ion chambers with a nafion separator. The Scintrex 209 was the preferred tritium meter for CANDU facilities, while improvements on the model were done via the Scintrex 309, Overhoff 750SB and the BotP300. Real-time tritium monitors with improved sensitivity, gamma compensation and radioactive gas compensation would enable workers to assess tritium hazards quicker. The three competing technologies for real-time measurement of tritium in air at the moment are ionization chambers, proportional counters and scintillation-based detectors. The most promising of these technologies described by Wood and Surrette is a device based on ionization chambers, consisting of three chambers, separated by different absorbers. The center chamber and the top chamber are separated by a thin

sheet of aluminum, and center chamber is separated with a sheet of aluminized mylar from the bottom chamber. Sample gas is drawn through the center chamber which detects all beta energies while medium and high energy betas are detected in the bottom chamber and only high energy betas are detected in the top chamber. Air-flow scintillation counters have had problems with sensitivity and are limited by the effective surface area of the scintillators used. Increasing the surface area does not solve the problem because it decreases the response time for the detection of HTO. Air-flow proportional counters have yielded promising results however the design of such detectors may be fairly complicated requiring temperature, humidity and pressure compensation. All three methods require further investigation and research [5].

As research on the three techniques continues, other techniques concerning tritium detection were also investigated.

A paper in 2003 by W.M.Shu, M.Matsuyama, T. Suzuki and M.F Nishi [10] discussed an investigation dealing with tritium process monitoring detecting bremsstrahlung X-rays. The investigation explained using the characteristics of a tritium process monitor detecting bremsstrahlung X-rays with a sodium iodide scintillation counter with pure tritium in a concentration range of 10^2-10^8 GBq/m^3. The principle involved observing the bremsstrahlung X-rays generated by the interaction between beta particles from tritium and a gold film coated on the inner surfaces of a small measuring cell. The sensitivity of the monitor was determined to be about 0.5 GBq/m^3/cpm in this concentration range with a linear response being determined between the counting rate of the bremsstrahlung x-rays and tritium. Comparing this value to the Derived Air Concentration (DAC) of tritium, which was found to be $3.0x10^5$ Bq/m^3 [5], this value is approximately 1560 DAC.

According to the paper, ionization chambers suited to online and real-time tritium monitoring could monitor tritium concentrations in a wide range from extremely low to significantly high levels. The disadvantage of such chambers is that they are easy contaminated and difficult to decontaminate. In addition to developing this process monitor however, testing for traces of Helium release from a Uranium bed for tritium storage was also determined and the results were successful. The monitor is able to trace the percentage of He-3 in the gases released from a bed in real time when the total pressure is smaller than 10^3 Pa. The paper concluded that the process of detecting bremsstrahlung x-rays would provide a promising tritium monitor for the fuel processing system of fusion reactors [10].

From these papers it is possible to conclude that each innovation has its advantages as well as disadvantages and it is important to take these into consideration when building a detector for a defined and particular purpose.

In more recent developments, tritium monitoring has been under investigation by the CANDU Owners Group (COG) and was discussed at the 2010 Information Systems on Occupational Exposure (ISOE) North American ALARA Symposium/EPRI Radiation Protection Conference [11]. A presentation by A.C Vikis discussed the main objectives of ongoing research and development projects and internal dosimetry regarding tritium exposure was specifically included. This type of research evaluates the prospect of developing a biological based personal dosimeter for tritium. The research so far includes potential methods to measuring tritium in the form of HTO vapor. The research concluded that a personal tritium monitor capable of detecting exposures of 100 μSv cannot presently be constructed [11].

Other types of research involved evaluating the relative contribution of organically bound tritium to total tritium dose. Such research is important because it may lead to a detector being developed capable of measuring tritium in a CANDU power plant where workers may have to work in high energy gamma fields. Although ALARA principles of decreasing the dose by shielding, distance and time limit exposure to such fields seem adequate, an internal exposure of tritium can be substantially hazardous due to organically bound tritium.

Results presented by Vikis included organically bound tritium contributing up to 20% of the total tritium dose to members of the public, aquatic animals and plants. A tritium suit is also under development with an HTO vapor protection factor which reduces worker dose at the reactor face by 10 times the dose which is in accordance with ALARA as required by radiation protection regulations. Two suits are said to be under research, one incorporating a self-contained air purification system and a second with an air purification system in a transportable suitcase. The presentation also highlighted that a compatible commercially available wireless communication system has been identified and successfully tested for application with these suits [11].

This research and presentation supports the objective of this thesis and highlights the importance of measuring tritium as well as its contribution to the safety of nuclear energy workers.

1.3 Outline of Thesis

This thesis will cover the effect of gamma radiation and beta particles on plastic scintillators and conclude with the feasibility of building a detector that is capable of

measuring tritium in high energy gamma backgrounds. Chapter 2 will cover the background needed to understand the principles of gamma and beta detection as well as mixed field dosimetry regarding dual/mixed radiation detection. It will provide a concise explanation that will help in formulating the necessary hypothesis for the experimental work conducted as well as the expected outcomes of the simulated data. Chapter 3 discusses the experimental setup of the detector that was built as well as the scintillation material chosen and its properties. It will discuss the problems encountered during setup and the resolutions determined. Chapter 4 discusses the results obtained from the gamma sources and will include different trials of each isotope while emphasizing their agreement to a pre-determined hypothesis. Fe-55 and Cs-137 will be discussed in further detail to highlight the deviation from the hypothesized results. It will also discuss the results obtained from trials with a beta source and the problems encountered with their interaction with plastic scintillators. Following these results, the chapter will outline the three different hypotheses that were determined and will be compared to the results obtained from experimental data. The difficulties of working with plastic scintillators when dealing with beta particles will also be addressed. The last section of Chapter 4 includes an MCNP simulation of H-3 beta particles that solidify the calculated hypothesis for H-3 beta particles to determine the possibility of building a tritium detector. The MCNP simulation is explained in detail with the outcome in relation to the calculations done prior to the simulation being analyzed. Chapter 5 will address future developments and the application of this body of research to these potential paths. The conclusion following Chapter 5 will summarize research methods and the development of techniques over the course of this investigation. The conclusion will also finalize the discussion

regarding the feasibility of building a personal tritium monitor and will discuss subsequent detectors that may use this research in developing additional detectors required in CANDU reactor power plants.

Chapter 2: Background to Theory

2.1 Interaction of Gamma Rays with Matter

High energy gamma rays in nuclear environments can be common and potentially harming to workers present. These rays originate inside the nucleus of an atom rather than from the electrons surrounding the nucleus as is the case of X-rays. They are an energetic form of electromagnetic radiation and are a product of radioactive atoms. When a nucleus is in an excited state, it may emit packets of electromagnetic radiation called photons. The emission of these photons does not alter the number of protons or neutrons in the nucleus and are simply the product of transition to a lower energy state inside the nucleus of an atom. When an emission takes place the ray has only energy, is mass-less and is highly penetrating.

Radiation may be absorbed, transmitted, emitted or scattered. Absorption takes place when incoming radiation passes through a material and gets completely absorbed allowing no detection on the other side. Transmitted radiation is not absorbed but passes through and can be detected on the other side. This means that that the material is effectively transparent to the transmitted radiation. Incident radiation is scattered when it exits at a different angle as when it entered. There may be some absorption as well. If incoming radiation is absorbed or the intensity of the incoming radiation decreases in mass while the rest goes through the material, it is termed as attenuation and is the most prevalent for gamma radiation [3].

The attenuation of gamma radiation relies on the energy of the incoming radiation, the type and mass of the material through which the radiation passes.

Attenuation of beta and alpha radiation rely on definite ranges and can be completely absorbed at times, but incident gamma radiation intensity decreases with increasing thickness of the absorber (material). The theoretical equation which determines this characteristic when good geometry is implemented as follows:

$$I = I_o e^{-\mu x} \quad [12, 13] \tag{2.1}$$

Where

I_o = gamma ray intensity at zero absorber thickness

x= absorber thickness

I = gamma ray intensity transmitted through an absorber of thickness x

e= base of natural logarithm system

μ= slope of the absorption curve = attenuation coefficient

Since the exponent term must be dimensionless, μ and x must have reciprocal units and in most cases where the x is in centimeters, μ is in centimeters^{-1}. μ is referred to as the linear attenuation (μ_l) coefficient, however if x is in g/cm^2 and μ is in (g/cm^2) $^{-1}$, then μ is referred to as the mass attenuation coefficient (μ_m). The relationship between the two types of coefficient may be represented as: $\mu_l(cm^{-1}) = \mu_l(cm^{-1}) * \rho(\frac{g}{cm^3})$ where 'ρ' is the density of the absorber [3].

The three methods of interaction of gamma radiation with an absorber or material with mass are important to understand. These include the Photoelectric effect, Compton scattering and Pair production.

The photoelectric effect is seen when an incident photon disappears entirely transferring its energy to a tightly bound electron of an atom in the material whose binding energy is

equal or less than the energy of the incoming photon. This photoelectron loses its kinetic energy in the material via two processes known as excitation and ionization. Ionization occurs when the photoelectron has sufficient energy to eject an orbital electron in an atom producing an ion pair. Excitation occurs when the energy imparted for ionization is insufficient and results in the orbital electron acquiring enough energy to jump to a higher energy orbital. De-excitation of this electron to a lower orbital can create characteristic radiation in the form of light. The photoelectric interaction is most prominent with atoms that possess a high atomic number 'Z' and photons with low energy [12,3].

The equation explaining the energy of the photoelectron is:

$$E_{pe} = hf - \emptyset \quad [3] \tag{2.2}$$

Where

h = plank's constant

f= frequency of the incident photon

ϕ=binding energy of electron

According to the equation, the energy of the photoelectron would be the incident photon energy minus the electron's binding energy.

Compton Scattering is different from the photoelectric effect because it is an elastic collision between a photon and an electron whose binding energy is much lower than the energy of the photon. The incoming photon collides with this "free" electron and transfers some portion of its energy to the electron along with a certain momentum. The incident photon is then scattered in a different direction with the residual energy. The incident photon then repeats the process albeit with a lower residual energy [12,3].

Due to energy and mass conservation, the energy of the scatter photon may be represented by the equation:

$$E' = \frac{E}{1+\left(\frac{E}{m_o c^2}\right)(1-\cos\theta)} \text{ [12]} \qquad (2.3)$$

Where

E'=Energy of scattered photon

E= Energy of incident photon

$M_o c^2$ = 511keV = rest mass energy of an electron

θ = the angle of scattering between the incident photon and scattered photon

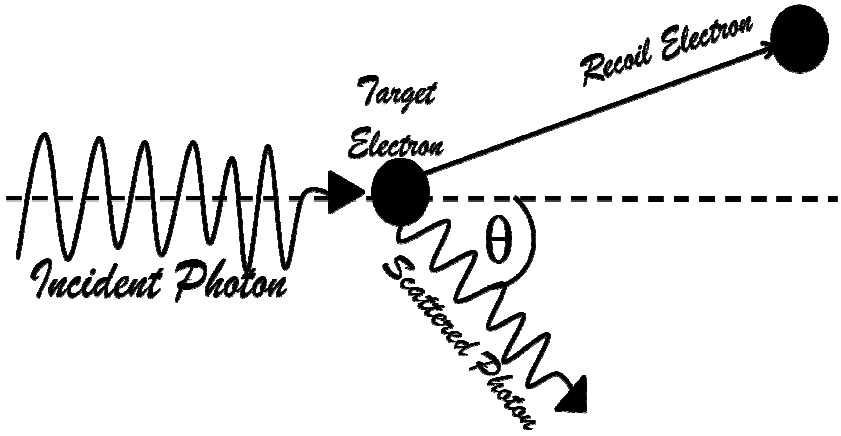

Figure 2.1: Visual Description of Compton Scattering

This process is most dominant among the three types of photon interaction at around photon energies of 1 MeV.

Pair Production is the third interaction for photons with matter and only occurs with photon energies beyond 1.022 MeV. This is due to the characteristics of the interaction and occurs when the photon passes within close proximity to the nucleus of an atom. The photon spontaneously disappears and its energy reappears as a positron and an electron

each with a rest mass of 0.511 MeV. This transformation from energy to mass must take place in close proximity to the nucleus. This is to conserve momentum due to the kinetic energy of the recoiling nucleus being small. Excess energy of photons possessing energies greater than the minimum needed to create the electron-pair is used as to project the electron-pair a certain distance within the material they are formed. This phenomenon may also occur near an electron, called triplet production, however the probability of such an event occurring is quite low in comparison to one occurring near a nucleus [12,3].

The cross-section of the production of a positron-electron pair occurring is proportional to Z^2+Z, where 'Z' is the atomic number of the absorber and is therefore important for high-atomic numbered absorbers. The cross section increases slowly with increasing energy between the threshold of 1.02 MeV and 5 MeV[12]. For higher energies, the cross-section is proportional to the logarithm of the quantum energy. This increasing cross-section accounts for the increasing attenuation coefficient for high-energy photons [12].

After the electron pair is produced, it is projected forward with a certain kinetic energy, lost by excitation, ionization and bremsstrahlung. When the positron has exhausted all of its energy it may combine with an electron and in the process produce two photons each with energy of 0.51 MeV[12,3]. These photons now undergo photoelectric Compton scattering depending on the absorber.

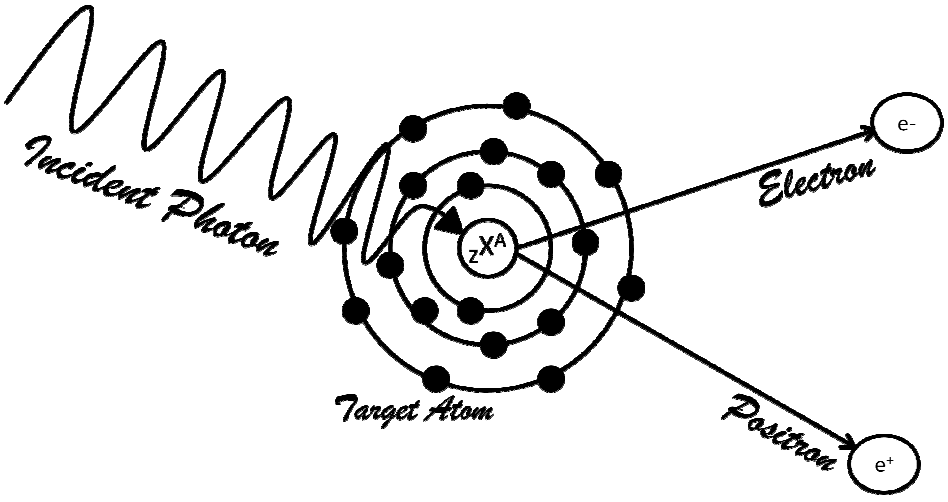

Figure 2.2: Visual Description of Pair Production

Differentiating between the three interactions and the conditions under which each would occur can be illustrated with Figure 2.3. The x-axis of the graph is the energy of the photon, while the y-axis represents the atomic number of the absorber. For each photon interaction with an absorber, the most probable interaction can be determined from the graph.

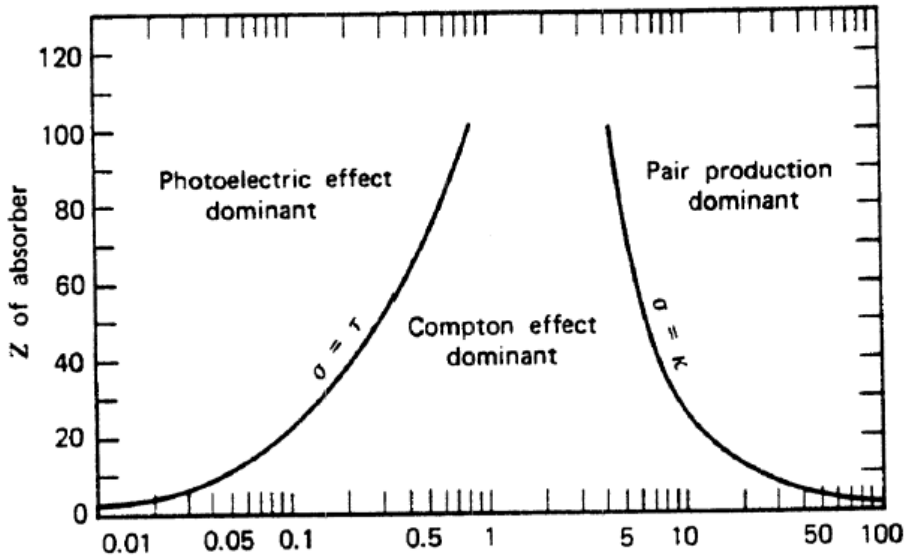

Figure 2.3: Plot to differentiate between the occurrences of the three gamma interactions [2]

2.2 Interaction of Beta Particles with Matter

Beta particles are essentially electrons and hence have the same mass as orbital electrons. This makes them susceptible to deflections during collisions and therefore very hard to track as they go through a torturous path. Beta particles lose their energy via ionization, excitation and bremsstrahlung[12]. The interaction between the electric field of a beta particle and the orbital electrons of the absorbing medium leads to electronic excitation and ionization. These interactions are referred to as inelastic collisions. The electron is held in the atom by electrical forces and the energy is lost by the beta particle in overcoming these forces. Electrical forces act over long distances, the collision between a beta particle and an electron occurs even though the particles do not come into actual contact. The energy lost by the beta particle depends on its distance of approach to the electron and on its kinetic energy [12].

The energy lost by the beta particle can be represented by the equation

$$E_k = E_t - \varphi \quad [12] \tag{2.4}$$

Where

E_k= Kinetic energy of ejected electron

E_t =Energy lost by the beta particle during the collision

φ=ionization potential of the absorbing medium

An ion pair is produced in some cases, while in others the ejected electron has sufficient kinetic energy to produce a small cluster of several ionizations. The ejected electron may also receive a considerable amount of energy, causing it to travel a long distance and leave a trail of ionizations. This is a 'delta ray' electron [12]. The bremsstrahlung

interaction occurs when a beta particle passes close to a nucleus and the strong Coulomb forces causes the beta particle to swerve sharply from its original path. The change in direction is termed radial acceleration and the beta particle loses energy by electromagnetic radiation at a rate proportional to the square of the acceleration. This is in accordance with Maxwell's classical theory [12].

Another important aspect for beta particles is their range. The attenuation of beta ray by any given absorber may be measured by interposing successively thicker absorbers between a beta-ray source and a suitable beta-ray detector and counting the beta particles that penetrate the absorbers. It was found that the beta-particle counting rate decreases rapidly at first and then slows as absorber thickness increases. Eventually a thickness of absorber is reached that stops all beta particles. The observed limit point, beyond which there is no further decrease in the counting rate of the absorption curve, is the range of the beta rays in the material of which the absorbers are made [12, 4, 3]. The range for beta particle can be determined by the equation

$$R\left(\frac{mg}{cm^2}\right) = 412E^{1.265-0.0954lnE} \quad [12] \qquad 0.01 \leq E \leq 2.5\text{MeV} \qquad (2.5)$$

Dividing the range by the density yields the thickness the absorber needs to be to stop all beta particles emitted from the source.

2.3 Scintillation Detection

Having discussed the interaction of radiation with matter and specifically the case of beta radiation, it is essential to understand the type of matter that the radiation would interact with. For this research, the solid state matter making up the detector is the Scintillator.

Scintillation detection refers to the ionizing radiation that is detectable based on light generation. Scintillation is one of the oldest techniques on record for measuring ionizing radiation. Many important aspects of scintillation detectors require consideration.

The main principles of scintillation material include converting kinetic energy of charged particles into detectable light with high scintillation efficiency while keeping the conversion linear. This means the light yield should be proportional to depositing energy over as wide a range as possible. The medium should also be transparent to the wavelength of its own emission for good light collection and the decay time of the induced luminescence should be short so that quick signal pulses can be generated. The material should also be of good optical quality and be manufactured in sizes large enough to be of interest to a practical detector as well. The index of refraction should be near that of glass (approximately 1.5) to permit efficient coupling of the scintillation light to a photomultiplier tube or other light sensors [15, 4].

There is no scintillation material currently present that supports all factors, although compromise on some factors is acceptable based on the purpose of the scintillation material. Inorganic alkali halide crystals as well as organic-based liquids and plastic scintillators are the most widely applied scintillators [15]. The inorganic scintillators tend to have the best light output and linearity but are also susceptible to relatively slow response times. Organic scintillators are generally faster but yield less light. Both scintillators are purpose driven for different types of detectors. In the case of inorganic scintillators, the high Z-value of the constituents and high density of the inorganic crystals make it an ideal candidate for gamma-ray spectroscopy whereas organics are often preferred for beta spectroscopy and fast neutron detection [15, 4].

Since this thesis paper deals with measuring beta particles in a high-energy gamma background, it is ideal to use an organic scintillator such as a plastic scintillator for this purpose. Plastic scintillators are available commercially with a good selection of standard sizes of rods, cylinders and flat sheets. The material is relatively inexpensive and easy to handle. This makes it a practical choice for this research. The self-absorption of the scintillator light must be taken into consideration and attention should also be given to the attenuation properties of the material. Plastic scintillators consist of a solid solution of organic scintillating molecules in a polymerized solvent. For organic scintillators such as anthracene, stilbene and many of the commercially available liquid and plastic scintillators, the response to electrons is linear for particle energy approximately above 125 keV. The response to heavy charged particles such as protons or alpha particles is always lower for equivalent energies and is nonlinear at much higher initial energies. Electrons and gamma rays are the only types of radiation of interest in this work and should produce a linear light output response [15, 4, 16].

Chapter 3: Experimental Set Up

3.1 Materials for Experimental Setup

The main task for the experiment was to construct a detector capable of detecting low energy beta particles in a high energy gamma background with the use of plastic scintillators. The components included an electrical box, plastic scintillators, a miniature photomultiplier tube, electrical connections, an oscilloscope, external voltage supply and integrated computer spectrometer software with a multi channel analyzer. The photomultiplier tube is essential to the system and will be explained in detail to understand how light generated by the scintillator is read as an output.

3.1.1 Photomultiplier Tube and Plastic Scintillators

The photomultiplier tube (PMT) chosen was the Hamamatsu R7400U which utilized the E5780 D type socket base. This is a subminiature tube regarded as the world's smallest photomultiplier tube assembly. It exhibits low noise and high gain and is suitable for photon counting applications [17].

Photomultiplier tubes consist of a photocathode region sensitive to ultraviolet, visible and near infrared regions of the electromagnetic spectrum. The first step of the PMT is to convert light photons into electrons. This process of photoemission occurs in three stages. The first is the absorption of the incident photon and transfer of an electron with the photo emissive material. The second is the migration of that electron to the surface and the third is the escape of that electron from the surface of the photocathode. This is all located inside a vacuum envelope where photoelectrons are emitted and directed by an appropriate electric field to an electrode (dynode). Secondary electrons are

now emitted at this dynode for each impinging primary photoelectron. These secondary electrons in turn are directed to a second dynode and so on until a final gain of approximately 10^6 is achieved. The electrons from the last dynode are collected by an anode which provides the signal current that is read out [18]. Figure 3.1 illustrates this process.

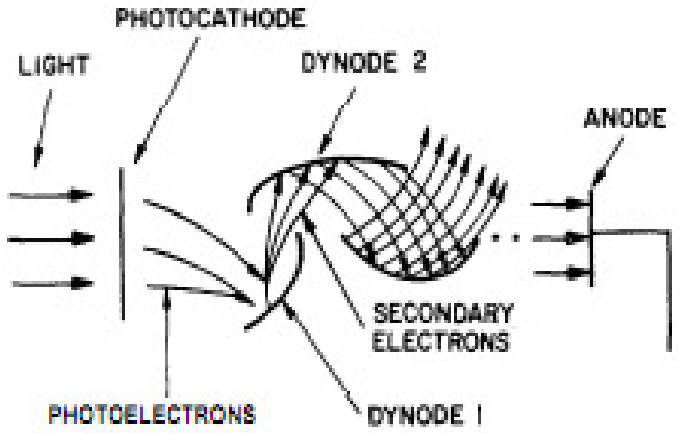

Figure 3.1: The process inside a PMT [35]

One of the most important components of a PMT is the sensitivity of its photocathode. When coupled with the use of scintillators, it is traditional to quote overall photocathode efficiency in terms of current produced per unit light flux on its surface. This is noted as quantum efficiency of the photocathode [12, 17].

It is defined as $$QE = \frac{number\ of\ photoelectrons\ emitted}{number\ of\ incident\ photons} \qquad (3.1)$$

The ideal photocathode would retain a quantum efficiency of 100%; however a more practical scenario shows the maximum quantum efficiency to be between 20 and 30% [17]. The R7400U PMT that was used shares this efficiency and features a 16mm diameter and a 12 mm seated length. It has an 8-stage electron multiplier composed of metal channel dynodes and has an excellent response time with a rise time of 0.78 ns [17]. The E5780

PMT base that was used along with the PMT needed a negative high voltage for which an external power supply was used. The base required three wires to be properly connected to the necessary inputs and outputs. One of the wires, the cathode, required grounding while another was used to provide the input voltage signal connected via an SHV cable. The third wire was connected to the output via a BNC connector enabling the signal to be sent through to the preamplifier. The maximum high voltage that was applied to the PMT at all times was 800 V. The schematic of the PMT base is given in Figure 3.2, while the schematic of the set up is given in Figure 3.3.

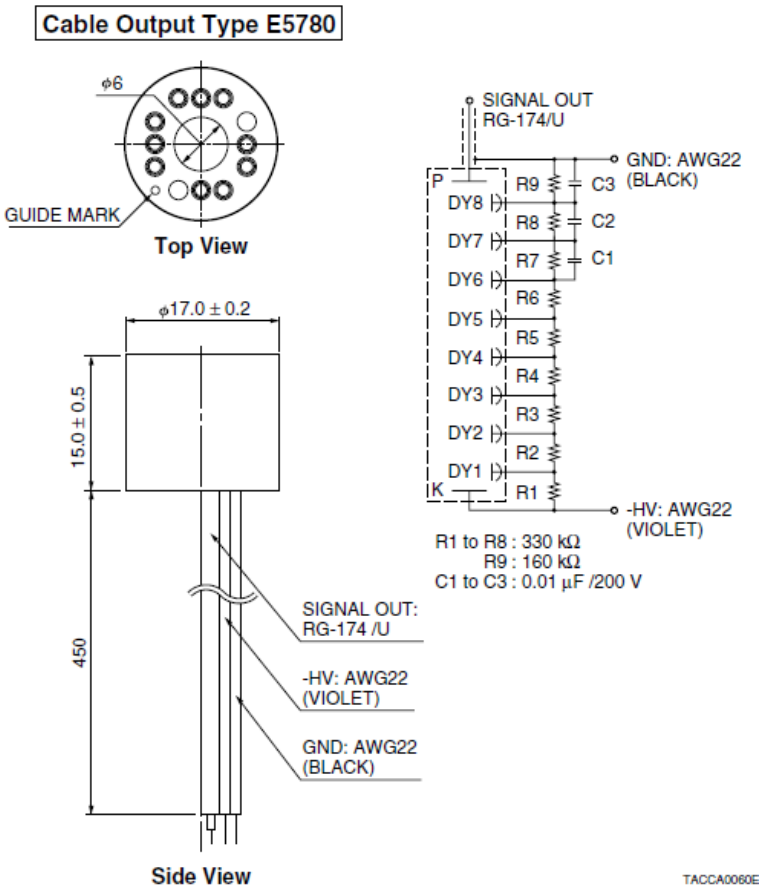

Figure 3.2: Schematic of a Photo Multiplier Tube

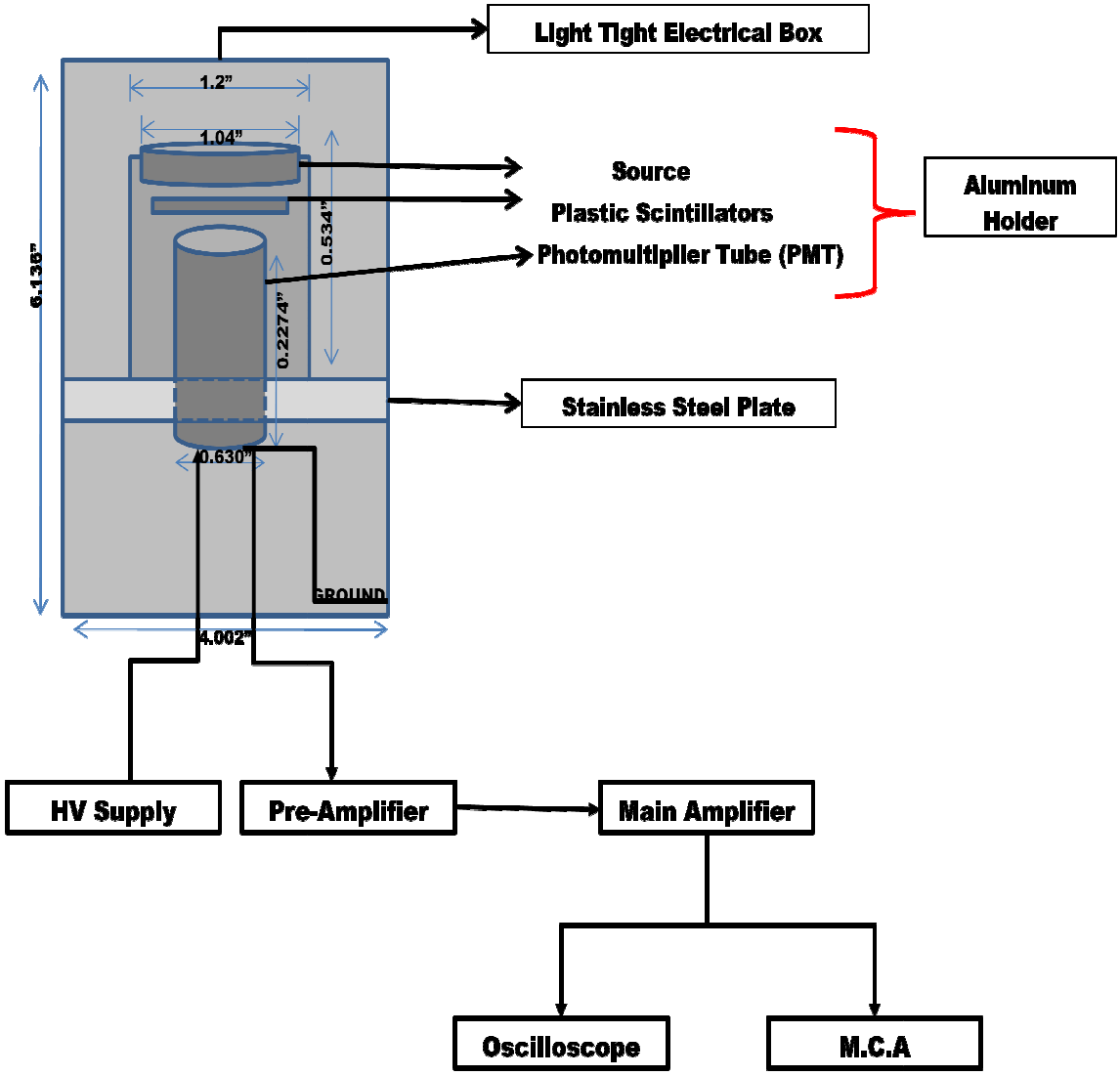

Figure 3.3: Schematic of Experimental Setup

The BC-400 series plastic scintillator from Saint Gobain Crystals and EJ-212 series plastic scintillators from Eljen Technologies were chosen for these experiments. Both the EJ-212 and the BC-400 series plastic scintillators are used for general purpose type scintillators and are sensitive to both gamma photons and beta particles. Both scintillators share properties such as the light output being 65% Anthracene with the

wavelength of maximum emission being 423 nm and the decay constant being 2.4 ns. The refractive index is also shared for both scintillators and is 1.58 while the hydrogen to carbon ratio is 1.103. The density is minimally different where the BC-400 series plastic scintillators have a density of 1.032g/cm^3 while the EJ-212 series plastic scintillators have a density of 1.023g/cm^3 [19, 20] . After obtaining the plastic scintillators from Eljen Technologies, each thickness was measured 5 times with a micrometer to determine the uncertainty of the scintillator thickness. The results were the following:

Scintillator Thickness (mm)						
Trials	**0.05**	**0.250**	**0.50**	**1.00**	**1.50**	**2.00**
1	0.07	0.22	0.56	0.94	1.59	1.59
2	0.07	0.22	0.57	0.93	1.60	1.60
3	0.06	0.22	0.57	0.94	1.60	1.60
4	0.06	0.22	0.56	0.94	1.60	1.60
5	0.07	0.22	0.56	0.95	1.59	1.59
Average	0.06	0.22	0.56	0.94	1.60	2.04
Deviation from Actual (%)	39.60	10.80	13.70	5.50	6.80	2.50

Table 3.1: Uncertainty Regarding Plastic Scintillator Thickness

3.1.2 Testing Chamber

The testing chamber consisted of a light tight electrical box with a stainless steel mount to allow for easy changing of the plastic scintillators and the sources without disturbing the electrical connections within the box. On the top of the stainless steel mount, a cylindrical aluminum holder was constructed for proper alignment of the PMT,

scintillators and the source. The holder supported the PMT at one end and the source was placed at the other end with 5mm spacing between the plastic scintillators, which were placed directly onto the well of the PMT with the electrical box mounted vertically using two wooden planks at right angles and desk clamps to hold the weight of the box steady onto a lab table (refer to figure 3.7). The box was then fitted with a high voltage and signal output cable connected directly to the multichannel analyzer card via SHV connections. The lid would seal shut using a single clamp and then tightened (refer to figure 3.7). To minimize scattering, optical grease was applied onto the well of the PMT and the scintillators. The optical grease was purchased from Eljen Technologies and had a refractive index of 1.47 [21]. The EJ-550 Optical Grade Silicon Grease was very effective in enhancing the results obtained for each trial.

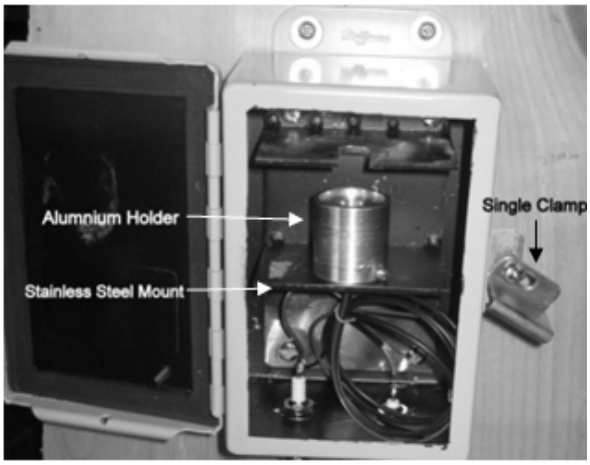

Figure 3.4: Inside view of electrical box

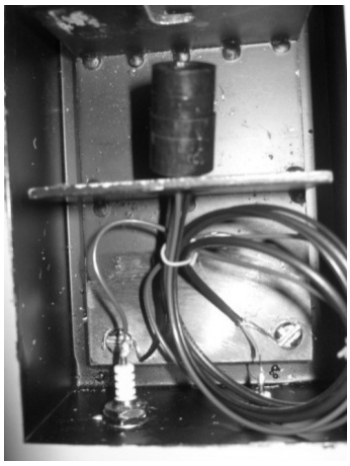

Figure 3.5: PMT and base connections

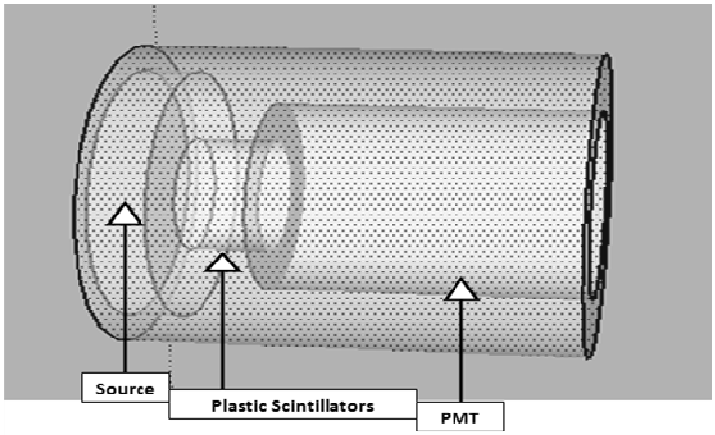

Figure 3.6: Aluminum holder shown in Google Sketch

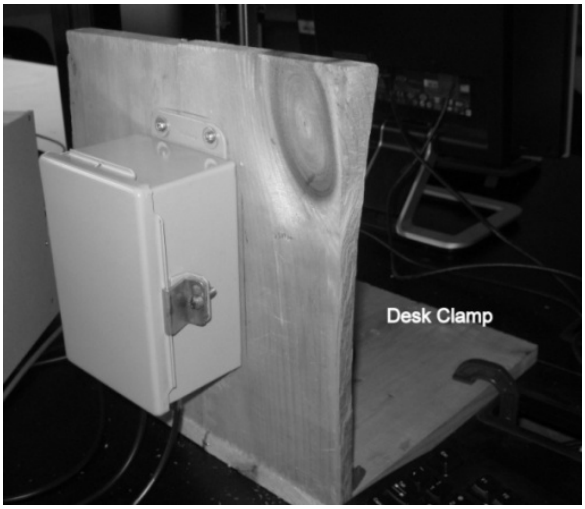

Figure 3.7: Electrical Box Supported by Wooden Boards Attached by Desk Clamps

When connections to the detector were made, an external amplifier, preamplifier and an external voltage source were connected via the following schematic:

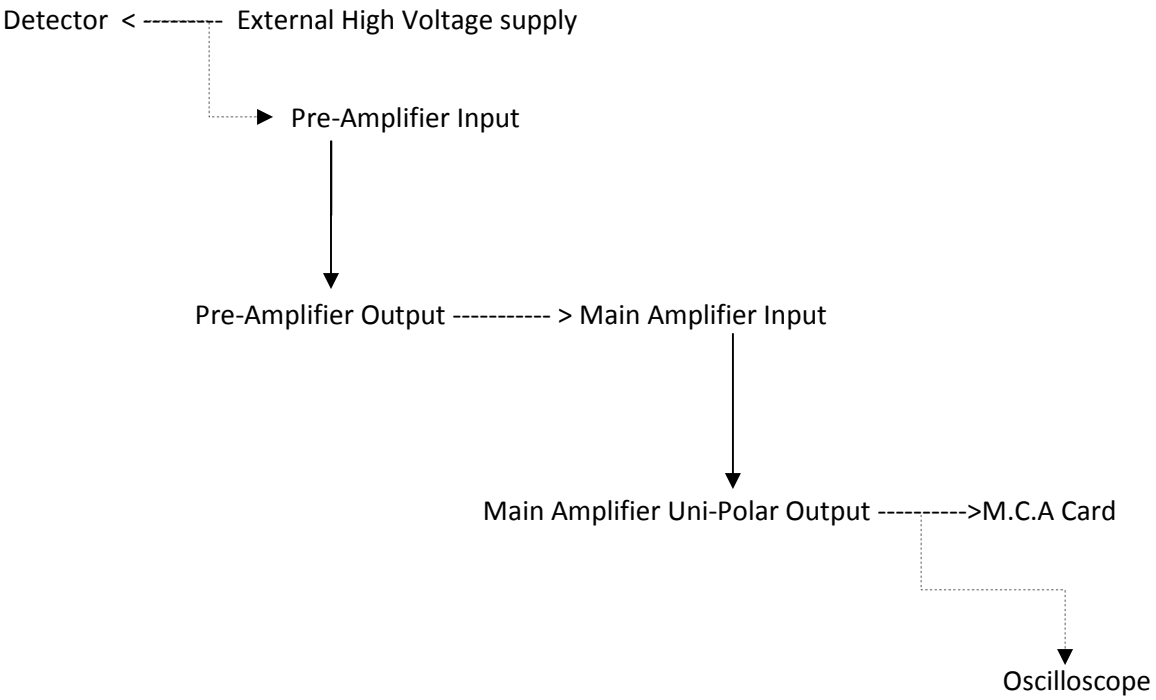

The connection to the detector also accounted for noise generation by the system which meant that the total gross counts were recorded above a lower-level discriminator (LLD) setting that ensured dead-times of less than 10% for all measurements. The LLD was set to 10 and the upper level discriminator (ULD) was set to 100 (in percentage of the number of channel numbers present) [22].

3.1.3 Accounting for Uncertainty:

The uncertainty in the system was tested before measurements were taken to account for the error with each measurement. The systematic uncertainty was ascertained by taking one source and one plastic scintillator and running ten trials while keeping all other parameters constant. Each time, the entire assembly was taken apart, including the

plastic scintillator being taken out of the well of the PMT and the optical grease wiped off the face of the PMT and reapplied each time. The source was also positioned back into its aluminum slot for each run. This was done with a 500 μm scintillator and a Cs-137 source while the run time stayed the same at 600 seconds (10 mins) with the gain of 15. All results presented for this thesis incorporate a subtraction in background counts.

Trial	**1**	**2**	**3**	**4**	**5**	**6**	**7**	**8**	**9**	**10**
Counts	883217	837198	869896	881507	872325	874701	866619	880526	886146	875143
Average			**Standard Deviation**				**Systematic Error**			
872727.8			**13926.6**				**1.6**			

Table 3.2: Systematic Error for Data Set 1

The Systematic Error was calculated by the following formula:

$$Systematic\ Error = \frac{Standard\ deviation}{Average} * 100 = \frac{13926.6}{872727.8} * 100 = 1.6 \qquad (3.2)$$

To reconfirm consistency of the systematic error, another set of trials was done with a Co-60 source and a plastic scintillator of 2500 μm at a run time of 600 seconds and a gain of 15. The results were as follows:

Systematic Error for Data Set 2										
Trial	1	2	3	4	5	6	7	8	9	10
Counts	126946	126518	121377	122833	129993	124967	126976	124726	123366	124484
Average			**Standard Deviation**				**Systematic Error**			
125218.6			2478.4				2.0			

Table 3.3: Systematic Error for Data Set 2

The second data set yielded a systematic error of 2.0%, while the first data yielded an error of 1.6%. The two sets were averaged to give a systematical error of 1.8%. The

statistical error was established by calculating the square root of the counts themselves, and finding the percentage of that amount relative to the initial integrated counts. An example of Co-60 has been given below:

Measurement Error of Data Set from Co-60 source									
Thickness	0	10	100	500	1000	1500	2000	2500	
Counts	4545	24769	34323	48957	60855	79320	102179	129993	
Square Roots of Counts	67.4	157.4	185.3	221.3	246.7	281.6	319.7	360.6	
Percentage	1.5	0.6	0.5	0.5	0.4	0.4	0.3	0.3	**Average of Percentage**
									0.6

Table 3.4: Measurement Error of Data Set from Co-60 Source

$$Percentage = \frac{Square\ Root\ of\ Counts}{Integraged\ Counts} * 100 \qquad (3.3)$$

The highest average of all the measurement error on the sets of data taken was rounded to 1%. Hence adding the 2.0% from the systematical error to the 1% from the statistical error we attain a total uncertainty of 3.0%.

The total uncertainty of the system is thus 3.0% for all integrated counts.

3.2 Simulation for MCNP

Determining the uncertainty of the system as 3.0%, helped validate the response obtained when measuring sources via this setup. However, an additional purpose of this research was to determine the feasibility of developing a tritium monitor for which a simulation was modeled. Calculations were also carried out to validate and compare the results obtained from the simulation. MCNP4a was used as the simulation tool for the

experiment. It is a computer code built and specifically designed for particle physics. MCNP stands for Monte Carlo N-Particle code and can be used for neutrons, photons and even electrons. It is based on the Monte Carlo code which was designed by Los Alamos during World War 2 [23]. The Monte Carlo algorithm selects a particle at random and calculates the energy of its interaction with all other particles. It randomly displaces the particle and then calculates the energy of the interaction of the particle in its new position with all other particles. The MCNP code was designed for applications such as radiation protection, dosimetry, radiation shielding, radiography, medical physics, nuclear criticality safety, detector design and analysis as well as nuclear oil well logging, accelerator target design, fission and fusion reactor design, decontamination and decommissioning. MCNP contains features that make it a useful tool in understanding the critical aspects of these applications. MCNP focuses on proper geometry and provides output tally plotters with variance reduction techniques. It has an extensive collection of cross-sectional data allowing probabilistic analysis primarily based on the Monte Carlo algorithm [23,24] .

Due to all these features, MCNP4a was used for this research in light of the limitation of physical experimentation with tritium. MCNP 4a was used to simulate the range of beta particles, specifically the number of tritium beta particles that would interact with the scintillator over a five minute period. This was done by building a simple setup which tallied the number of beta particles reaching the PMT. The source was defined as a volumetric source surrounding the PMT inside a given volume. The number of H-3 beta particles detected would then be compared to the number of high

energy gamma photons recorded in an identical 5 minute period which was determined experimentally.

The MCNP simulation was set up as the following:

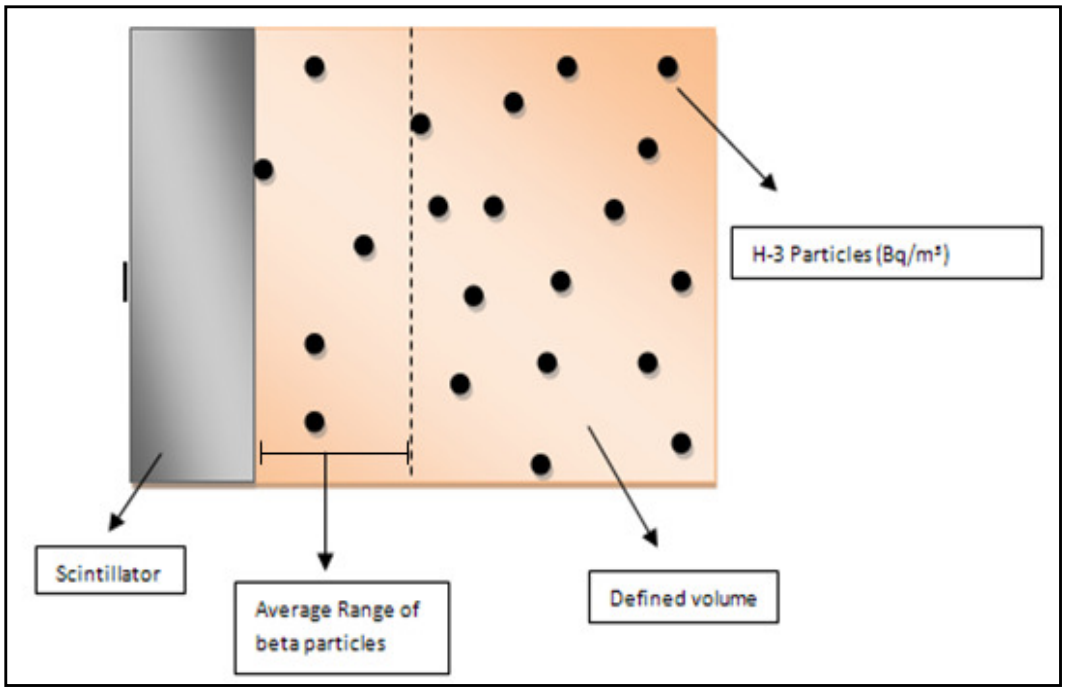

Figure 3.8: MCNP Simulation

The results of the simulation will then be used to calculated analytical values to assess the possibility of using this research to build a tritium monitor capable of operating in a high energy gamma backgrounds.

Chapter 4: Results/Discussion of Experimental Work

4.1 Gamma Sources

After the detector had been built, each source was counted as the scintillator thickness was increased. The four gamma sources that were used are listed in table 4.1 in the order of increasing energy. The attenuation coefficients were obtained from the Handbook of Health Physics and Radiological Health, Third Edition.

Isotope	Energy (MeV)	Attenuation Coefficients (cm^{-1})
Fe-55	0.0059	23.025
Am-241	0.0595	0.255
Cs-137	0.662	0.108
Co-60	1.332	0.079

Table 4.1: Attenuation Coefficients of Gamma Sources Used based on Increasing Energy [26]

As shown in Table 4.1, Fe-55 emits photons with the smallest energy and possesses the greatest attenuation coefficient while Co-60 emits photons with the highest energy and possesses the smallest attenuation coefficient. These attenuation coefficients were found for polyvinyl-toluene which is the material composing the BC-400 and EJ-212 series plastic scintillators [20]. Equation 2.1 predicts Iron-55 would have a very steep slope on a graph of increasing scintillator thickness versus the number of counts obtained at each thickness as compared to the other gamma sources. As further scintillation material is placed in front of the photocathode, more photons from the source are attenuated by the material allowing the photocathode to collect light photons and register more events from the scintillator. Since Fe-55 has the highest attenuation coefficient, the amount of scintillation material needed to attenuate these photons would be minimal in

comparison to the amount of material needed to attenuate Co-60 or Cs-137 photons. This implies that the amount of scintillator material needed to attenuate photons from a source is exponentially realated to the attenuation coefficient of the source, and the attenuation coefficient depends on the energy of the source.

As previously mentioned, the plastic scintillators used for the gamma sources were purchased from Saint Gobain Limited with material thicknesses measured at 10 μm, 100 μm, 500 μm, 1000 μm, 1500 μm, 2000 μm and 2500 μm. Background counts were noted at approximately 300 counts over 5 minutes.

4.1.1 Overall Results of Gamma Sources

Each trial was run for 600 seconds (10 minutes) at an external gain of 15 (course gain: 30, fine gain: 0.5) and at a voltage of 800 V. Two data sets were recorded to observe the consistency and accuracy of each set of counts. The second set was used in constructing graphs for analytical purposes. All scintillator thicknesses are measured in micrometers and thicknesses of 0μm indicate counts observed without any scintillation material.

Result Set For Gamma Photons								
Fe-55								
Scintillator Thickness	0	10	100	500	1000	1500	2000	2500
Counts (Trial 1)	6,253	53,730	196,649	546,373	542,105	397,843	346,224	272,502
Counts (Trial 2)	5,120	56,822	222,713	631,757	647,041	475,944	300,856	240,196
Am-241								
Scintillator Thickness	0	10	100	500	1000	1500	2000	2500
Counts (Trial 1)	4,740	13,913	37,690	156,956	298,621	468,313	650,047	841,639
Counts (Trial 2)	5,120	13,983	38,771	155,340	325,908	472,686	599,846	852,820

Cs-137 (with 0.125mm copper disk in between the source and the scintillators)								
Scintillator Thickness	0	100	500	1000	1500	2000	2500	
Counts (Trial 1)	3013	65908	83095	98614	120074	147950	179560	
Counts (Trial 2)	Note: Only 1 data series was taken with Cs-137 source with a 0.125mm copper disk in between source and scintillator							
Co-60								
Scintillator Thickness	0	10	100	500	1000	1500	2000	2500
Counts (Trial 1)	5,533	23,595	35,649	43,460	60,274	82,650	103,587	137,924
Counts (Trial 2)	4,545	24,769	34,323	48,957	60,855	79,320	102,179	129,993

Table 4.2: Result Set For Gamma Photons

The results from the gamma sources were in good agreement with the expected relationship between integrated counts and scintillator thickness and are shown graphically in Figure 4.1 and Figure 4.2.

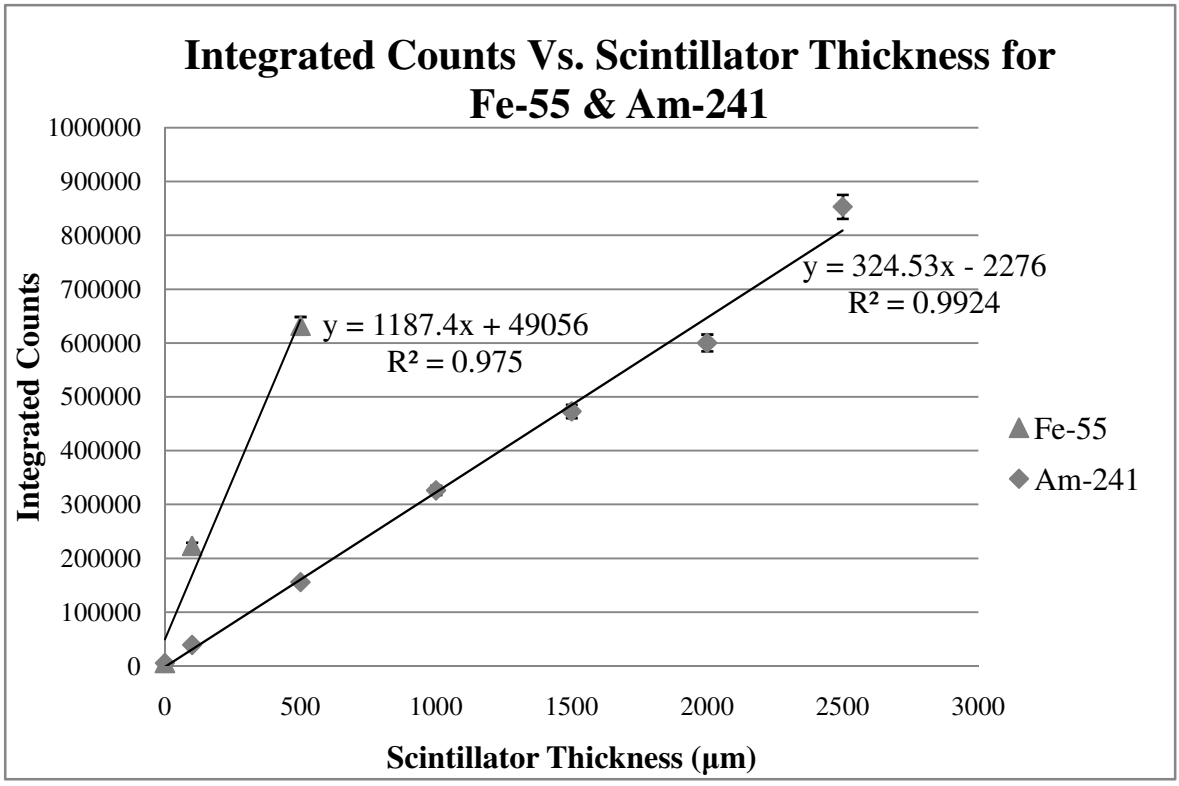

Figure 4.1: Plots of Fe-55 and Am-21 gamma sources versus increasing scintillator thickness

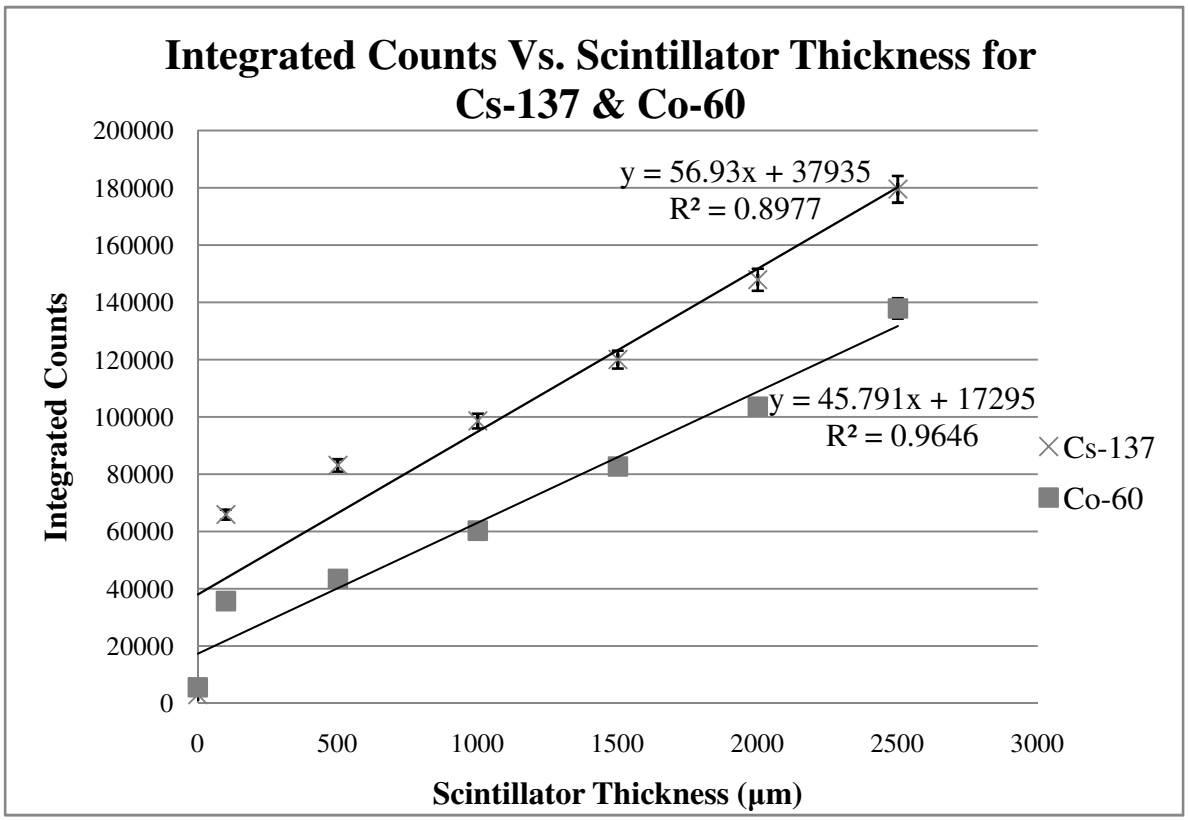

Figure 4.2: Plots of Cs-137 and Co-60 gamma sources versus increasing scintillator thickness

A line of best fit was plotted through each point for each source and the results produced show an increasing linear trend as the thickness of the scintillator increases. The total uncertainty on each of these points was around 6.0%. The measurements were taken without a scintillation material to form a baseline and then again with the thicknesses mentioned in the last section. As predicted the Iron-55 resulted in the highest slope of 1187, followed by Am-241 with a slope of 324, Cs-137 with a slope of 57 and with Co-60 with a slope of 46.

4.1.2 Cs-137 Measurement Difficulties

A note should be made regarding the Cs-137 which initially resulted in extremely high counts being registered. This was due to Cs-137 being a mixed gamma and beta source. Cs-137 emits 662 keV gamma photons as well as beta particles with a maximum energy

of 512 keV with a probability of 0.946 [29]. Due to this characteristic of the source, the beta particle emissions needed to be blocked with a copper disk. The disk was inserted between the source and the plastic scintillator to absorb the beta particles that were being emitted from the source. The gamma photons passed through, thus contributing to the counts measured by the multi channel analyzer. Initially an arbitrary thickness of 1mm copper disk was used to block the beta particles emitted from the source which resulted in a significant decrease in the number of counts for each thickness. A calculation was then done to determine the proper thickness of copper that should have been used to block the number of beta particles being emitted by the source. Using equation 2.5, the range of beta particles emitted from the Cesium can be determined and was found to be 0.17 g/cm^2.

$$R\left(\frac{mg}{cm^2}\right) = 412E^{1.265-0.0954lnE} \tag{4.1}$$

$$= 412(0.512)^{1.265-0.0954\ln(0.512)}$$

$$= \frac{169.26mg}{cm^2} * \frac{1g}{1000mg} = \frac{0.1693g}{cm^2}$$

Once the range of the beta particles is found, the subsequent step is to determine the amount of copper needed to stop the particles.

Assuming the density of Copper to be 8.94 g/cm^3 [27]

$$\frac{Range}{Density} = \frac{0.1693g}{cm^2} * \frac{cm^3}{8.94g} = 0.018cm * \frac{10mm}{cm} = 0.18mm \tag{4.2}$$

Cesium-137 Trial To Reduce Beta Particle Counts								
Cs-137 (no copper disk in between)								
Scintillator Thickness (µm)	0	100	500	1000	1500	2000	2500	
Counts	149,452	775,915	837,198	854,802	997,853	1,060,760	1,204,959	
Cs-137 (with 1mm copper disk in between the source and the scintillators)								
Scintillator Thickness (µm)	0	10	100	500	1000	1500	2000	2500
Counts	512	7,071	12,475	22,222	32,433	48,477	63,105	84,139
Cs-137 (with 0.125mm copper disk in between the source and the scintillators)								
Scintillator Thickness (µm)	0	10	100	500	1000	1500	2000	2500
Counts	3013	65908	12,475	83095	98614	120074	147950	179560

Table 4.3: Cs-137 Trials to reduce Beta Particle counts

Therefore, the amount of copper needed to stop the beta particles emitted from Cs-137, would be 0.18 mm. A copper piece with the closest thickness to this amount was obtained at a thickness of 0.125 mm and used for consequent trials. The result supported the hypothesis seen in Figure 4.4 while the counts using both disc can be seen in Table 4.2.

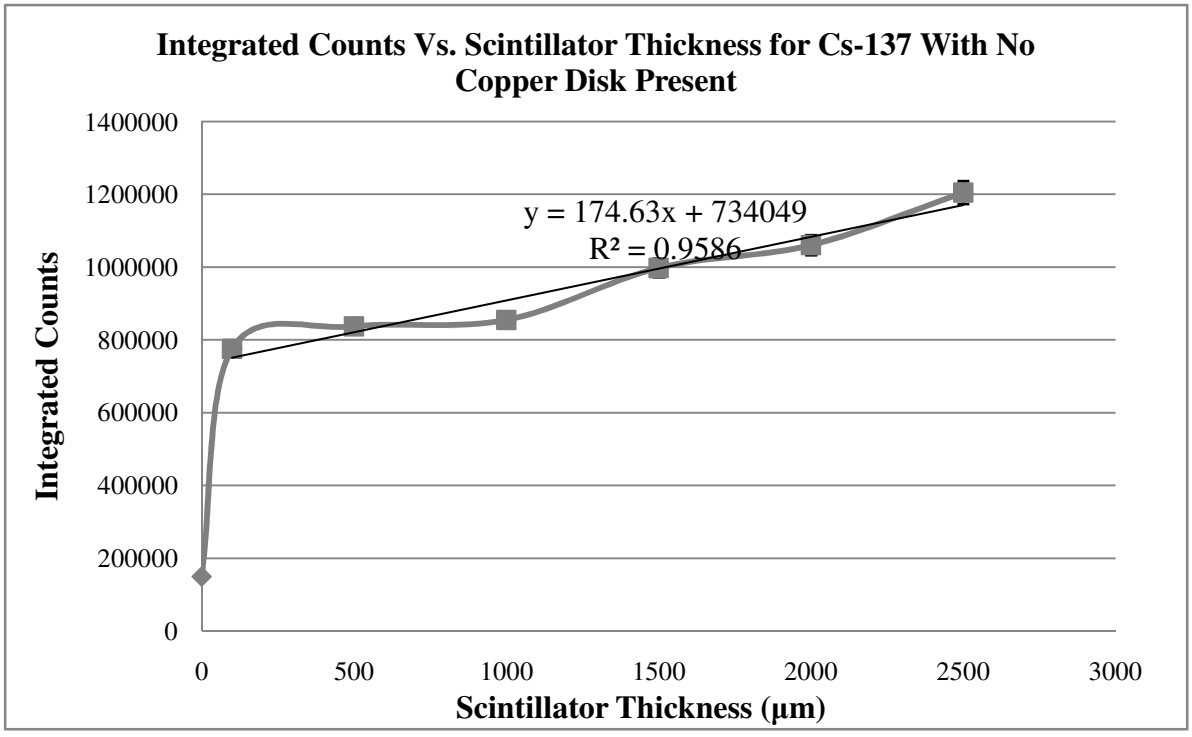

Figure 4.3: Cs-1376 Comparisons to Cut Down Beta Particles

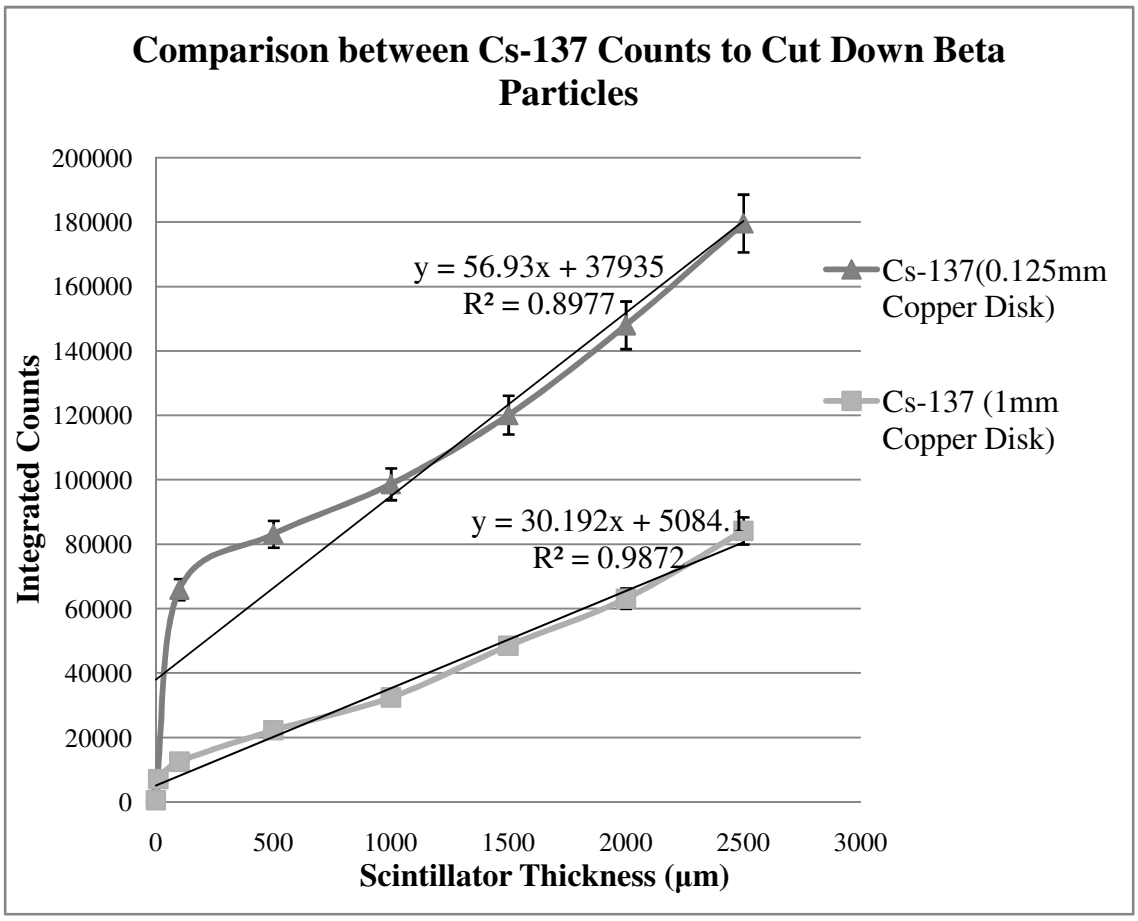

Figure 4.4: Cs-137 Comparisons between 1mm & 0.125 mm Copper Disks

As seen in Figure 4.3, without the copper disk the counts obtained from the Cs-137 source were substantially higher. It did not follow an increasing linear pattern which extended over the entire graph, however after a scintillator thickness of 500µm, an increasing linear trend was observed. Therefore if the beta particles were filtered, a linear trend should be confirmed. As seen in Figure 4.4, when a 1mm copper disk was used, the integrated counts were lower than the number of counts achieved without a filter. However the reduction in the counts was greater than expected when plotted on a graph of integrated counts versus increasing scintillator thickness, resulted in the slope of the plot being lower than that of Co-60. A third set of trials then utilized a 0.125 mm copper

disk since this was the closest thickness obtainable to the theoretical thickness of 0.178 mm. This thickness achieved a slope of 56, followed an increasing linear trend and supported the hypothesis of having the second smallest slope. The highest slope of Co-60 was shown in Figure 4.2 as being 46.

4.1.3 Iron-55 Results

One noticeable aspect of Figure 4.1 is the Fe-55 trend. It shows the counts measured for scintillator thicknesses varying from 0 µm to 500 µm. Scintillator thicknesses exceeding 500 µm were not added to the graph because the increasing linear trend does not apply beyond this thickness.

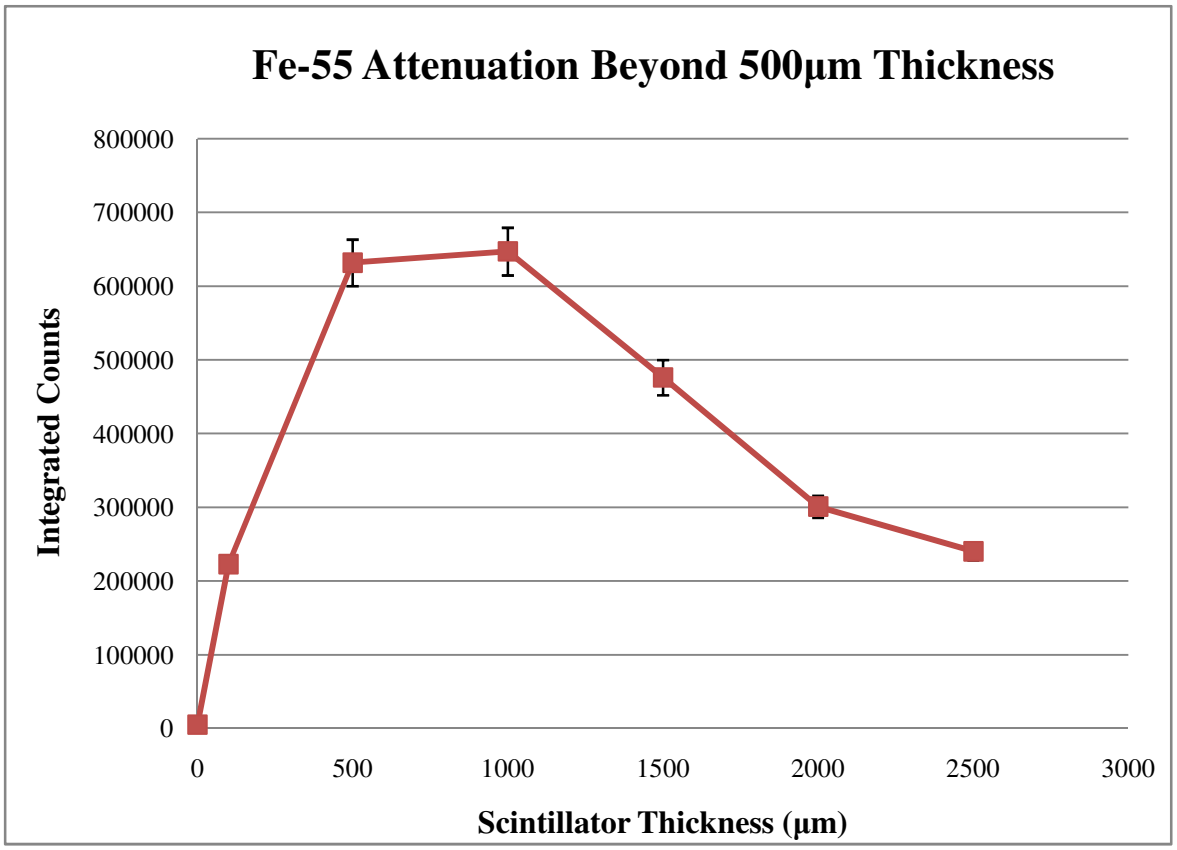

Figure 4.5: Fe-55 Attenuation beyond 500µm Thickness

Iron-55 is a source that emits low energy photons. Due to its high attenuation co-efficient, it produces a plateau followed by a decrease in the number of counts as scintillator thickness increases. Theoretically this can be explained via equation 2.1 presented in Chapter 2. Using the attenuation coefficient for Fe-55 from Table 4.1 and a thickness of 1000 μm, the number of attenuated photons emitted from the source at this thickness may be calculated as:

$$\frac{I}{I_o} = e^{-\mu x} \quad [13] \tag{4.3}$$

Where

$\mu = 23.0251 cm^{-1}$

$x = 0.1 cm$

$$\frac{I}{I_o} = e^{-(23.0251)*(0.1)} = 0.1$$

This 10% value represents the number of photons emitted from the source that have not been attenuated by the 1000 μm scintillator thickness. It also indicates that 90% of the photons emitted from the source have been attenuated. Once the majority of photons emitted by the source have been attenuated, any further addition of scintillator material may act as an obstruction in allowing the scintillator light photons to reach the photocathode due to internal scattering and absorption.

4.2 Nickel-63 Beta Source

The beta source used was a 1 μCi sealed source with a maximum energy of 65.87 keV and an average energy of approximately 17 keV. This average energy is approximately equal to the maximum energy of tritium beta particles of 18.6 keV [7].

From the given maximum energy of the beta particles that are emitted from the Ni-63 source, a maximum range can be found using equation 2.4, assuming the density of plastic scintillator to be 1.03 g/cm^3 [20].

$$R(\frac{mg}{cm^2}) = 412E^{1.265-0.0954lnE} \qquad 0.01 \leq E \leq 2.5MeV \qquad (4.4)$$

$$R = \frac{6.543mg}{cm^2} * \frac{0.001g}{mg} * \frac{1cm^3}{1.03g} = 6.345x10^{-3}cm = 63.45\mu m$$

The maximum range of the Nickel-63 beta particle is thus calculated at 64 μm. Based on the interaction of beta particles with matter, three different hypotheses were formulated prior to running the experiment. Figure 4.4 outlines the three scenarios. The first hypothesis was a gradual rise after the peak at the maximum established range for the Ni-63 beta particles. Scattering of light photons taking place inside the plastic scintillators would lead to a rise in the counts as the increasing amount of light reaching the photocathode would 'lift' very small pulse heights above the lower level discriminator increasing the number of integrated counts as the amount of scintillation material increases. The second scenario is the most intuitive which results in a rise to the maximum range for the Ni-63 beta particles followed by a plateau. At very small thicknesses of scintillator material, only part of a beta particles' energy is deposited in the scintillator which produces little light and contributes to pulses being below the lower level discriminator which in turn are not counted. At a scintillator thickness equal to the maximum beta particle range, all betas that can result in light pulses above the lower level discriminator will be counted. Beta particles are electrons and do not have an attenuation characteristic similar to photons. Any additional scintillation material added

beyond the needed thickness to register all the emitted particles would therefore have no effect on the outcome. Scenario three results in a rise to the maximum range of the Ni-63 beta particles followed by a gradual decrease in the number of counts registered as scintillation material is added. This may occur if a Ni-63 beta particle has reached its maximum range, and any additional scintillation material acts as an obstruction preventing light generated in the scintillator from reaching the photocathode.

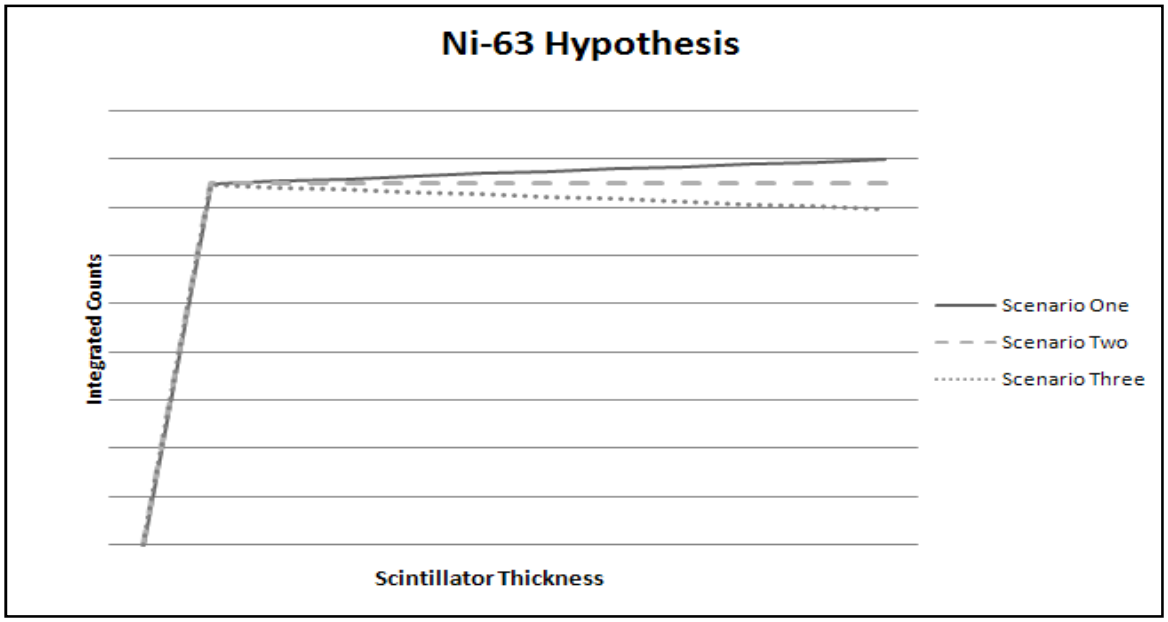

Figure 4.6: Hypothesized results for Ni-63

The initial results from Ni-63 posed many problems due to inconsistent results. Seven trials were conducted of which the first 5 are shown in Figure 4.7.

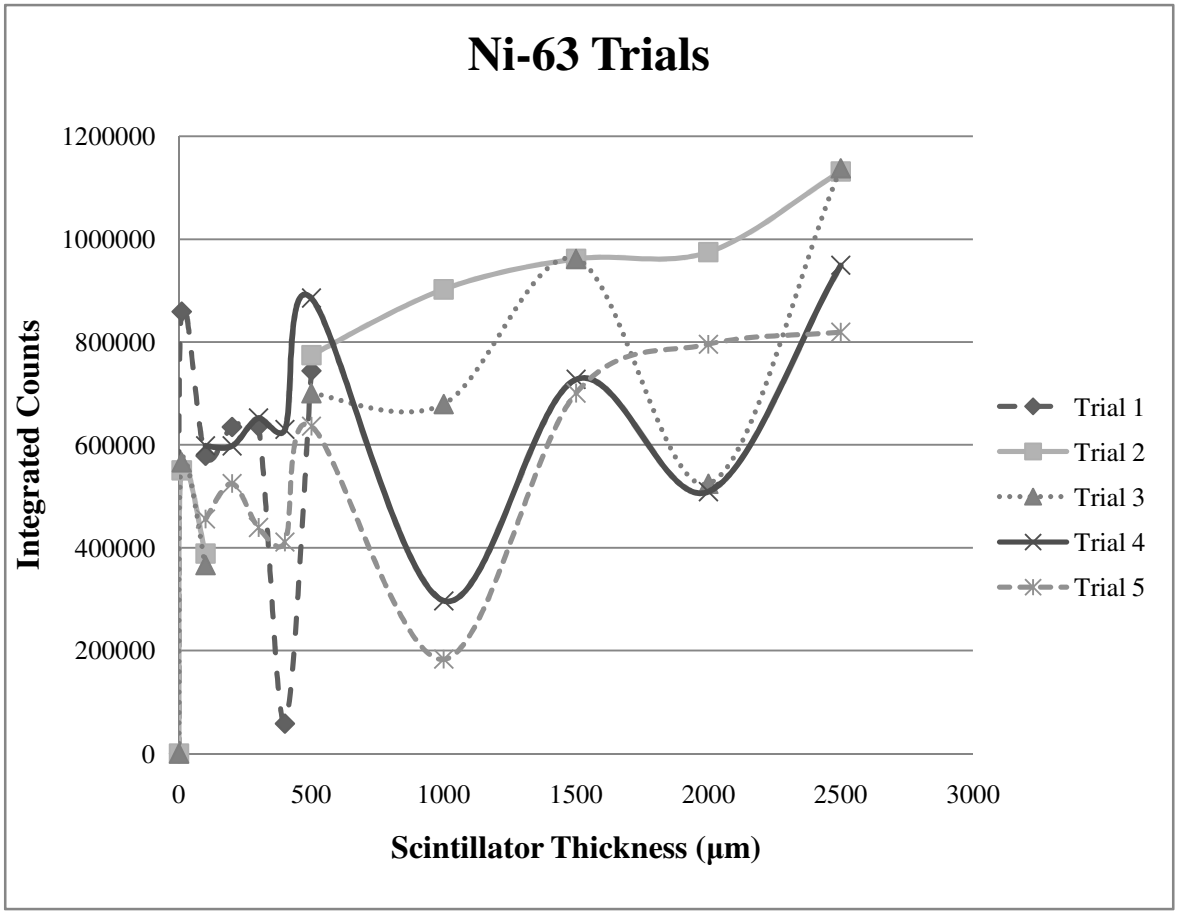

Figure 4.7: Ni-63 Initial Trials

The 5 trials from Figure 4.7 were initially conducted with no significant pattern to connect any of the three mentioned hypothesis. Several aspects of the setup were analyzed which yielded five additional trials. The final trial produced an improved pattern that supported one of the three hypotheses. This was achieved by segregating and analyzing three main aspects which proved to be significant when dealing with beta particles. These included the positioning of the scintillator, applying silicone grease and varying scintillator thicknesses. The positioning of the scintillator played a small role in the repeatability of each trial. Trials were done where the two faces of each scintillator disk were marked. The angle and the position at which the scintillator was in contact with the photocathode of the PMT were marked and recorded as well. This was done with tape

and markers and the result showed a slight variation which was within the acceptable range of error in the number of counts being measured under the same conditions.

Varying the scintillator thickness played a significant role in the repeatability and consistency of the counts. The BC 400 series plastic scintillators were used for the gamma sources. Stacking smaller thicknesses of scintillator material allowed thicknesses beyond 500 μm. This created discrepancies when working with the beta source because slight movements of each scintillator made a difference in recorded measurements. Hence the EJ-212 series plastic scintillators from Eljen Technologies were used to measure the Ni-63 beta particles. The EJ-212 series plastic scintillators were identical to the BC-400 series plastic scintillators with the exception of having specific dimension pieces matched to the thickness required for each trial. The sizes used to obtain a final measurement with the beta source were 50 μm, 100 μm, 250 μm, 500 μm, 1000 μm, 1500 μm, and 2000 μm.

The final improvement to the testing methodology was the application of silicone grease. This also made a significant change. The EJ-550 silicone grease was used as an optical coupling applied between the scintillation material and the photocathode. The purpose of optical coupling is to bridge the gap or boundary for light signals between different media. The refractive index measures the decrease in the speed of light inside that medium. The refractive index of the silicone grease used was 1.46 [21] as compared to the refractive index of the photocathode of the Hammatsu R7400U series PMT which is 1.49 [17]. A particular method used for the application of grease was found to be essential in achieving consistent results; a thick layer needed to be applied on the photocathode of the PMT. The scintillation disk must then be pressed evenly so as to avoid any air gap or air bubbles that might be present between the disk and the photocathode. The proper

application of the optical coupling creates a significant difference in the outcome and improves the repeatability of the system and the uncertainty of each trial. After running each trial five times while holding the conditions steady at an uncertainty of 3.0%, a new constant set of results was achieved for the Ni-63 source numerically in tables 4.4 and 4.5 and as well presented graphically in Figure 4.6. Each numerical set of results of Ni-63 at each thickness was averaged over 5 trials. Each trial was done over 5 minutes with the EJ-212 series plastic scintillators at 800 V, and an external gain of 15 (course gain: 30, fine gain: 0.5). The standard deviation and percent errors were also included with each set.

Table of Trials for Each Thickness for the Ni-63 Source								
50 µm								
Trial	1	2	3	4	5	**Average**	**St. Deviation**	**%Error**
Counts	465549	465615	464923	465739	465658	**465496.8**	**328.1**	**0.1**
100 µm								
Trial	1	2	3	4	5	**Average**	**St. Deviation**	**%Error**
Counts	485479	485642	488496	488349	488776	**487348.4**	**1640.3**	**0.3**
250 µm								
Trial	1	2	3	4	5	**Average**	**St. Deviation**	**%Error**
Counts	469657	471548	474031	474649	476058	**473188.6**	**2561.2**	**0.5**
500 µm								
Trial	1	2	3	4	5	**Average**	**St. Deviation**	**%Error**
Counts	458651	459472	461395	462442	464607	**461313.4**	**2377.6**	**0.5**
1000 µm								
Trial	1	2	3	4	5	**Average**	**St. Deviation**	**%Error**
Counts	431465	438726	440310	447366	444345	**440442.4**	**6056.5**	**1.4**
1500 µm								
Trial	1	2	3	4	5	**Average**	**St. Deviation**	**%Error**
Counts	410516	414335	417867	420351	420004	**416614.6**	**4165.5**	**1.0**
2000 µm								

Trial	1	2	3	4	5	Average	St. Deviation	%Error
Counts	392810	397539	403747	407480	407787	**401872.6**	**6535.4**	**1.6**

Table 4.4: Ni-63 Trials

Averaged Ni-63 Trials For Each Thickness							
Thickness (µm)	50	100	250	500	1000	1500	2000
Counts	465496.8	487348.4	473188.6	461313.4	440442.4	416614.6	401872.6

Table 4.5: Averaged Ni-63 Trials over each thickness and plotted in Figure 5

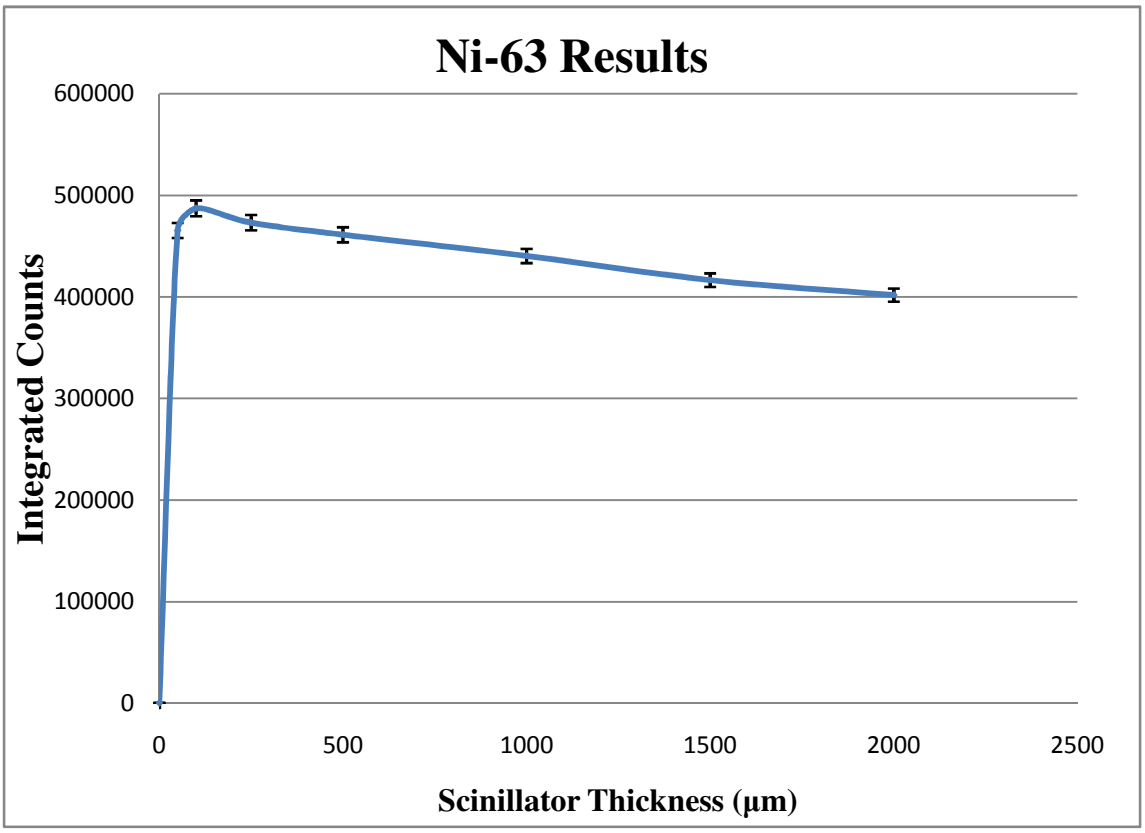

Figure 4.8: Ni-63 Results shown for integrated counts vs. scintillator thickness

The results from the experiment coincide with scenario three from the hypotheses, peaking at a scintillator thickness of 50µm followed by a constant decrease for additional scintillator thicknesses. At a 50µm thickness most of the beta particles have exhausted their range. Calculated previously, Ni-63 beta particles maintain a maximum range of

64µm. Since the thicknesses utilized for this experiment lacked 64µm, a peak was seen at a thickness closest to this maximum range. Additional scintillator thickness thus acts as an obstruction material for the amount of light reaching the photocathode and some light pulses would drop below the lower level discriminator for pulse height. This is similar to the Iron-55 trials for which extra scintillation material decreased the number of counts recorded by the PMT. It can be noted that in Figure 4.5 the decrease in counts for Fe-55 is steeper than that shown for Ni-63 in Figure 4.8. One explanation for this difference is the shape of the pulse-height spectrum for Fe-55 compared to Ni-63, Figures 4.10 and 4.17. For Fe-55 most of the counts are concentrated at smaller pulse-heights between the lower level discriminator and channel number 32, any loss of counts due to pulse-heights falling below the lower level discriminator setting will result in a greater proportion of counts lost compared to the maximum counts measured. This experimental work shows how beta particles interact with plastic scintillators and the important components required in obtaining accurate and consistent results.

4.2.1 Co-60 Trials with EJ-212 Series Plastic Scintillators

In order for a comparison to be made between the low energy beta particles from Ni-63 counts and the high energy gamma photons from Co-60 counts, another set of trials was obtained using the Co-60 source. These trails utilized the EJ-212 series plastic scintillators at the same thicknesses used for the Ni-63 trials. Each set of results at each thickness was averaged over 5 trials and was done over 5 minutes at 800V with an external gain of 15 (course gain: 30, fine gain: 0.5), similar to the Ni-63 trials.

Table of Trials for Each Thickness for the Co-60 Source								
50 µm								
Trial	1	2	3	4	5	**Average**	**St. Deviation**	**%Error**
Counts	23992	24211	24512	24337	24302	**24270.8**	**190.3**	**0.8**
100 µm								
Trial	1	2	3	4	5	**Average**	**St. Deviation**	**%Error**
Counts	24585	24889	24328	24406	24565	**24554.6**	**215.8**	**0.9**
250 µm								
Trial	1	2	3	4	5	**Average**	**St .Deviation**	**%Error**
Counts	27574	27654	27780	27568	28170	**27749.2**	**250.3**	**0.9**
500 µm								
Trial	1	2	3	4	5	**Average**	**St .Deviation**	**%Error**
Counts	31941	31515	31720	31787	31773	**31747.2**	**153.7**	**0.5**
1000 µm								
Trial	1	2	3	4	5	**Average**	**St .Deviation**	**%Error**
Counts	50194	50168	50212	50287	50432	**50258.6**	**106.6**	**0.2**
1500 µm								
Trial	1	2	3	4	5	**Average**	**St .Deviation**	**%Error**
Counts	62904	62657	62383	62378	62482	**62560.8**	**222.6**	**0.6**
2000 µm								
Trial	1	2	3	4	5	**Average**	**St .Deviation**	**%Error**
Counts	69304	69694	69691	69562	69129	**69476**	**250.6**	**0.4**

Table 4.6: Co-60 Trials

Averaged Co-60 Trials For Each Thickness							
Thickness	50	100	250	500	1000	1500	2000
Counts	24270.8	24554.6	27749.2	31747.2	50258.6	62560.8	69476.0

Table 4.7: Averaged Co-60 Trials over each thickness and plotted in Figure 5

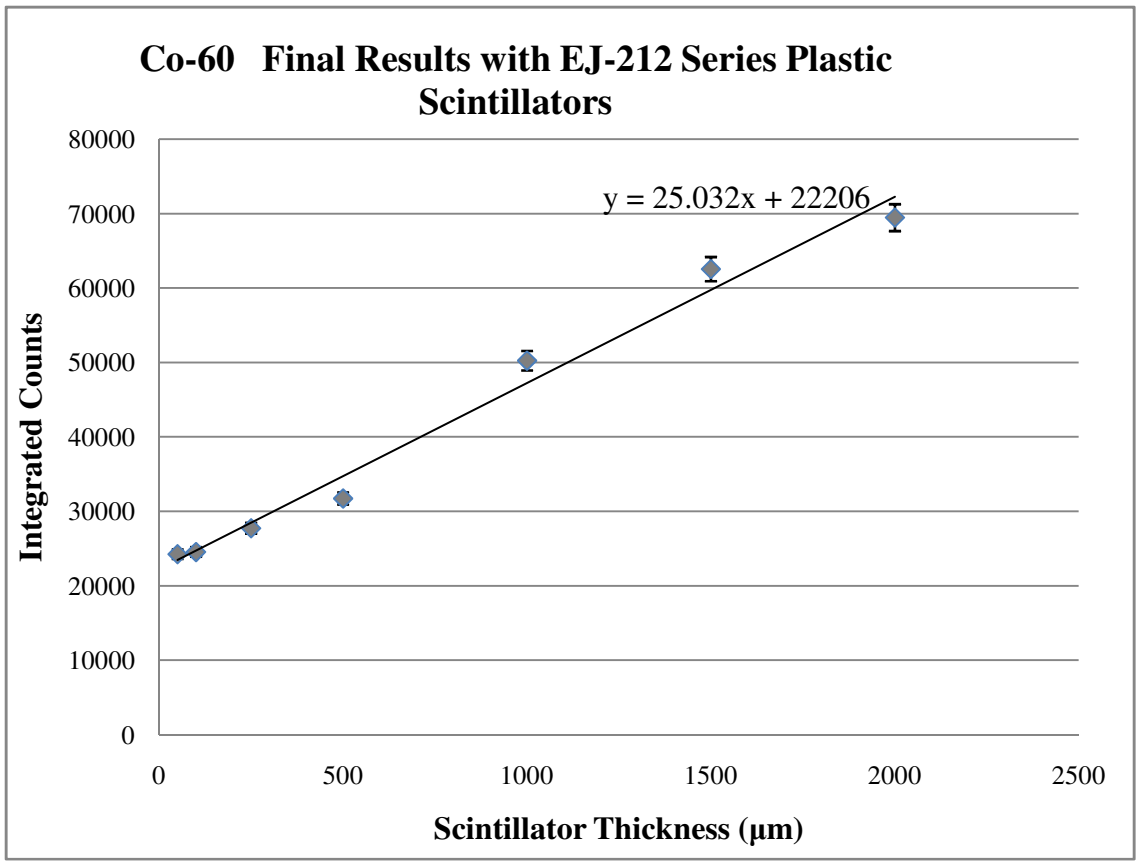

Figure 4.9: Co-60 Results for EJ-212 series plastic scintillators

4.3 Spectrum Analysis

It is important to understand the spectrum outputs in order to interpret the results from each trial correctly. Each pulse that is observed on the oscilloscope results in a count being registered through the multichannel analyzer. The channel number represents the pulse height in volts and is proportional to the energy deposited in the scintillator, while the number of counts at a given channel number represents the number of photoelectrons depositing that particular energy. Fe-55 emits low energy gamma photons which would predominantly undergo the photoelectric effect when interacting with matter. However a photo peak is not seen in the output due to two factors. The first is due to the light output for plastic scintillators. Both types of plastic scintillator have a

quantum efficiency such that 1MeV of deposited energy would generate on average 10,000 light photons [19]. Thus for sources such as Fe-55, which emit photons of approximately 5 keV, only 50 photons would be produced. Not all of these would be registered by the PMT, prompting an analysis of the PMT statistics as an important factor. This characteristic of plastic scintillators however, limits the observation of a photo peak for Fe-55 due to the scintillation efficiency being very low. The second factor involves the electron generation at the photocathode of the PMT being modeled as a fairly stochastic event. Due to the light output of the scintillator and the statistics of the PMT, a clear photo peak is not seen when counting the number of photons emitted from the Fe-55 source.

In the case of beta sources, each beta produces a pulse and the output is a count of how many beta particles reach the scintillator. This output is also influenced by the statistics of the PMT due to the number of light photons reaching the photocathode. Any decrease in the number of counts when measuring beta particles is thus due to extra material added between the source and the PMT, which attenuates the light photons reaching the photocathode of the PMT. In either case, the number of counts recorded by the multichannel analyzer is proportional to the number of photons or the number of beta particles that interact with the plastic scintillator. Although there are discrepancies with the energy of each photon being registered, the number of photon interactions is comparable to the number of beta interactions with the scintillator as the flaws regarding the statistics for the PMT are shared for both photons and beta particles. Below are the spectral outputs for each source measured at a thickness of 1000 μm.

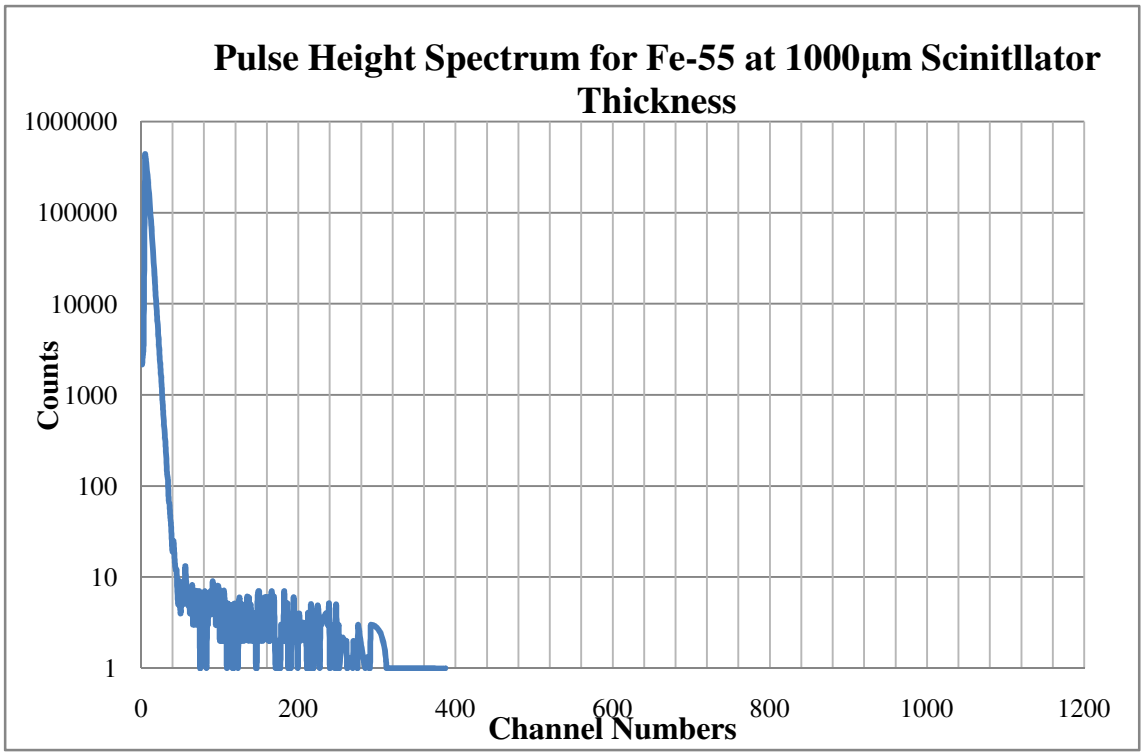

Figure 4.10: Iron-55 (Fe-55) Spectrum

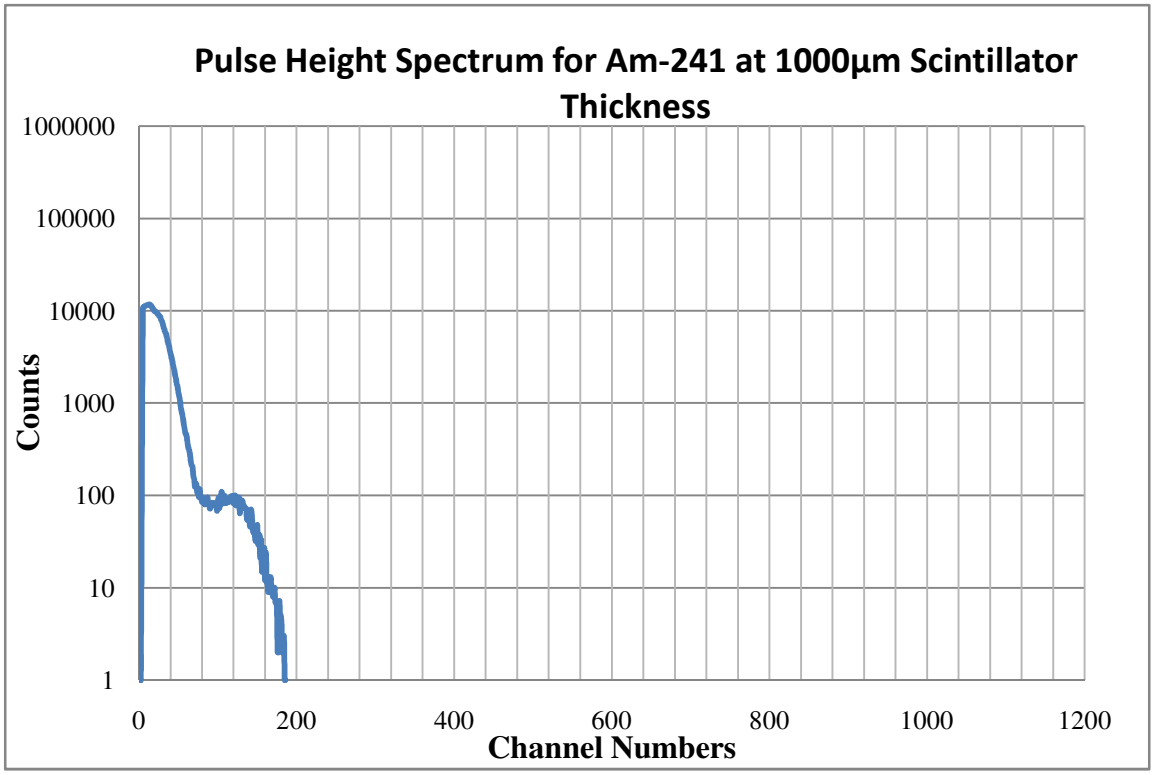

Figure 4.11: Americium-241 (Am-241) Spectrum

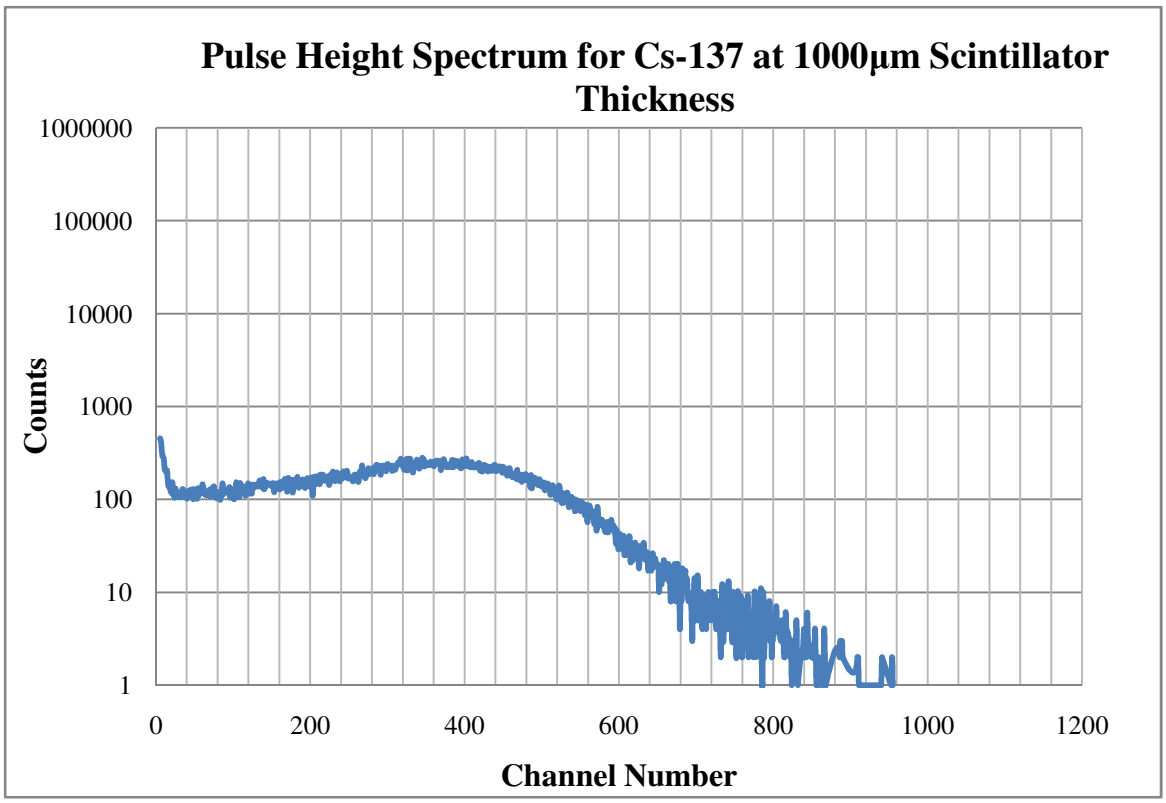

Figure 4.12: Cesium-137(Cs-137) Spectrum

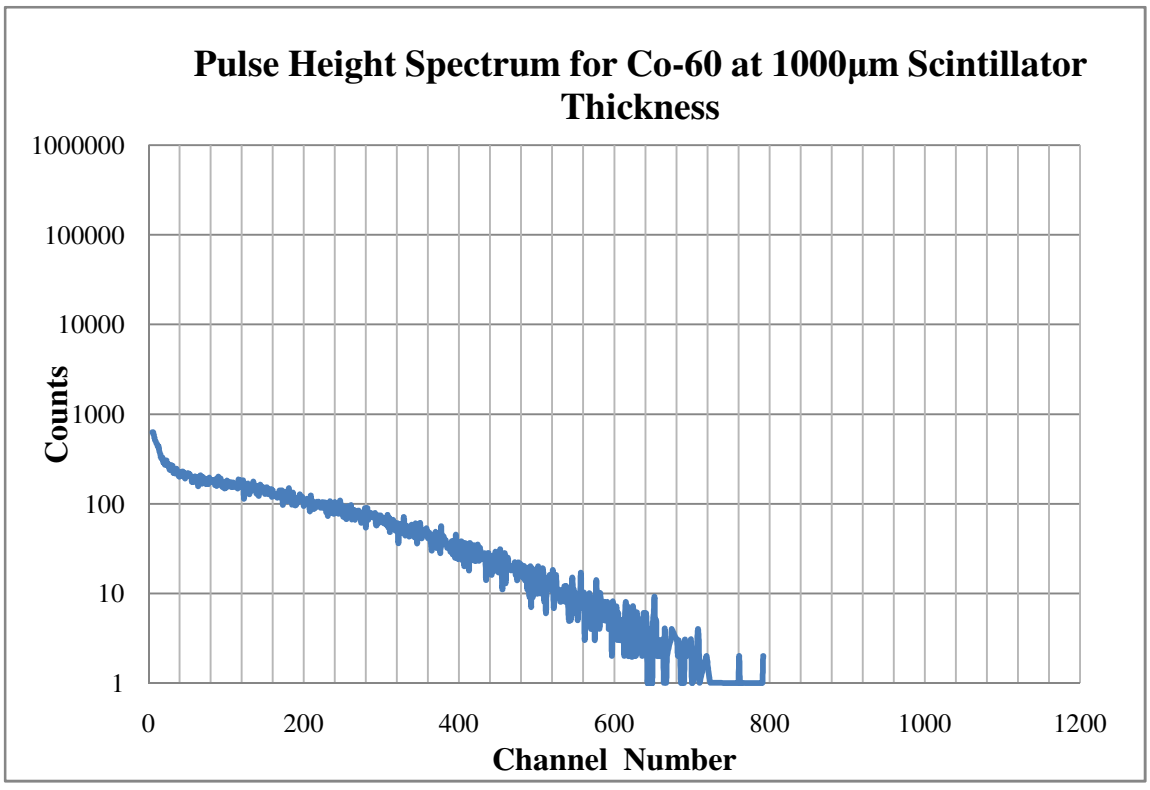

Figure 4.13: Cobalt-60(Co-60) Spectrum

4.4 Optimizing Scintillator Thickness

Optimizing the thickness of the scintillator is constrained by the need to be insensitive to high energy gamma photons with high penetration capabilities while being able to detect low energy beta particles. Gamma radiation ionizes indirectly while beta particles ionize directly and can be detected with minimal plastic scintillator thicknesses. The hypothesis for this work thus revolves around minimizing the scintillator thickness, allowing detection of most of the beta particles while allowing gamma photons to pass through the scintillation material undetected. After the analysis however, this hypothesis was proved incorrect due to three factors that were not taken into consideration. The first is identified by analyzing Co-60 counts being distributed differently over the range of pulse heights as the thickness of the scintillators increases. The distribution in the spectrum changes as the scintillator thickness changes. The second factor is derived by observing the Ni-63 counts which tend to decrease after a thickness of 60 μm instead of staying constant, while the third condition considers the absolute counts from the Co-60 source linearly increasing as the thickness in scintillator increases. To find the optimal scintillator thickness, Co-60 counts were compared to Ni-63 for each scintillator thickness, to find the highest ratio between the counts of the two sources.

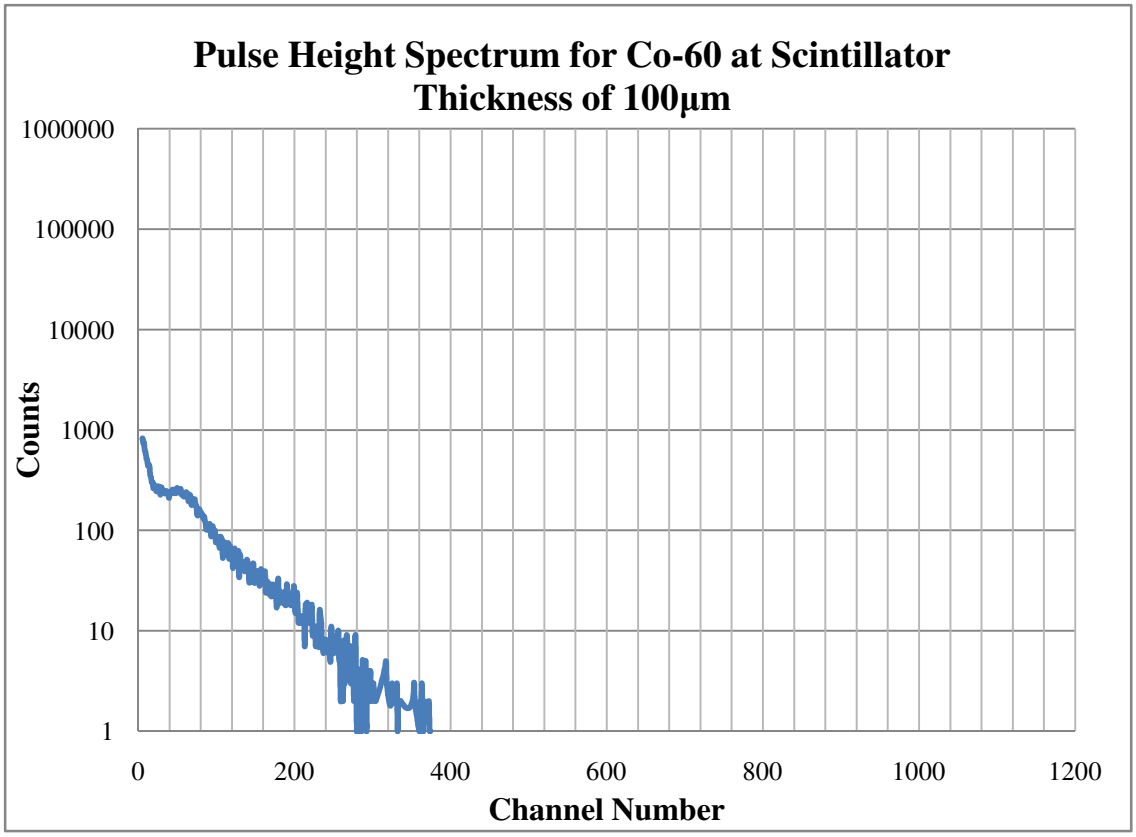

Figure 4.14: Co-60 counts at 100µm scintillator thickness

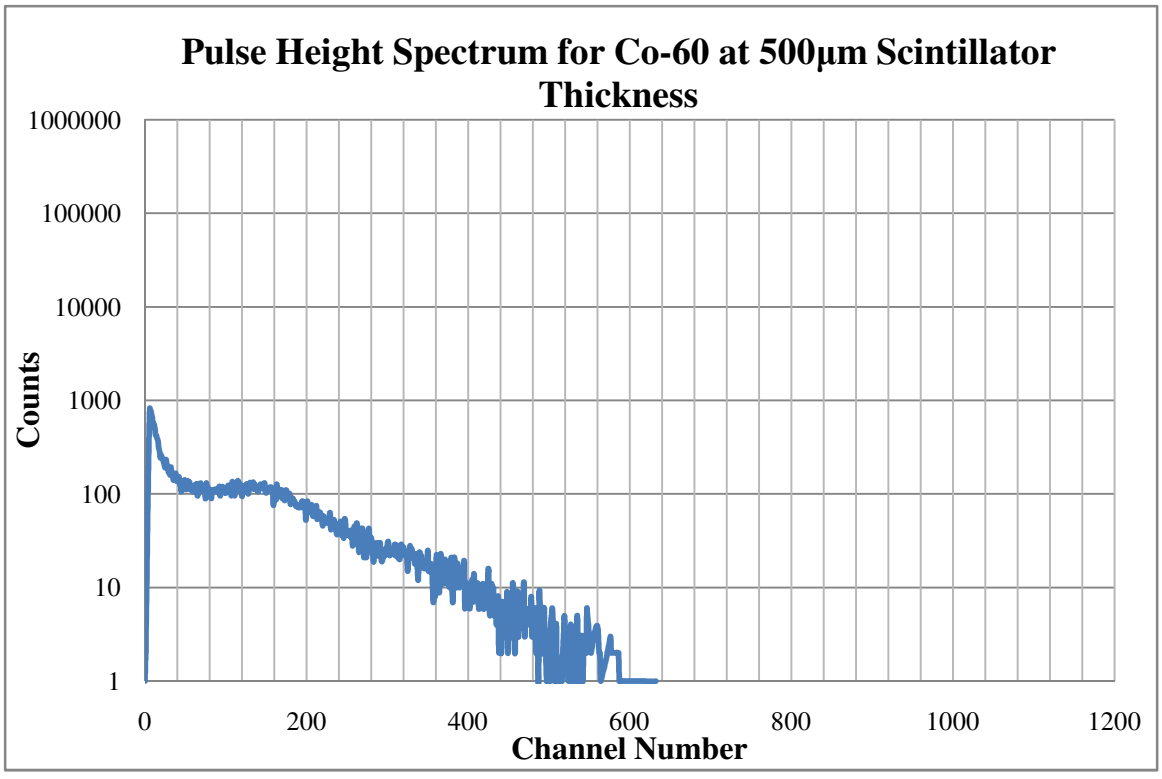

Figure 4.15: Co-60 counts at 500µm scintillator thickness

Figures 4.14 and 4.15 allow for comparisons between two trials measured for Co-60 at 100 μm scintillator thickness and 500 μm scintillator thickness. These two trials show how the pulse height spectrum shifts as the thickness of scintillator increases. Co-60 emits photons of energies at 1.332 MeV and 1.172 MeV, [7] which mainly interact through Compton scattering. Depending on the thickness of the scintillator, the incoming photons will either generate a single Compton electron with average energy and a range that is greater than the scintillator thickness, or will create multiple Compton electrons through more than one scattering interaction. In either case, it is expected that more electron energy would be deposited in the scintillator from a single photon interaction with increasing scintillator thickness. This increase in deposited electron energy per interacting photon will produce pulses of greater height. The pulse height spectrum is thus observed to extend to higher channel numbers with increasing scintillator thickness. These shifts in the pulse height spectrum pose a problem in determining optimal scintillator thickness since beta emitters result in a constant spread over the spectrum channels.

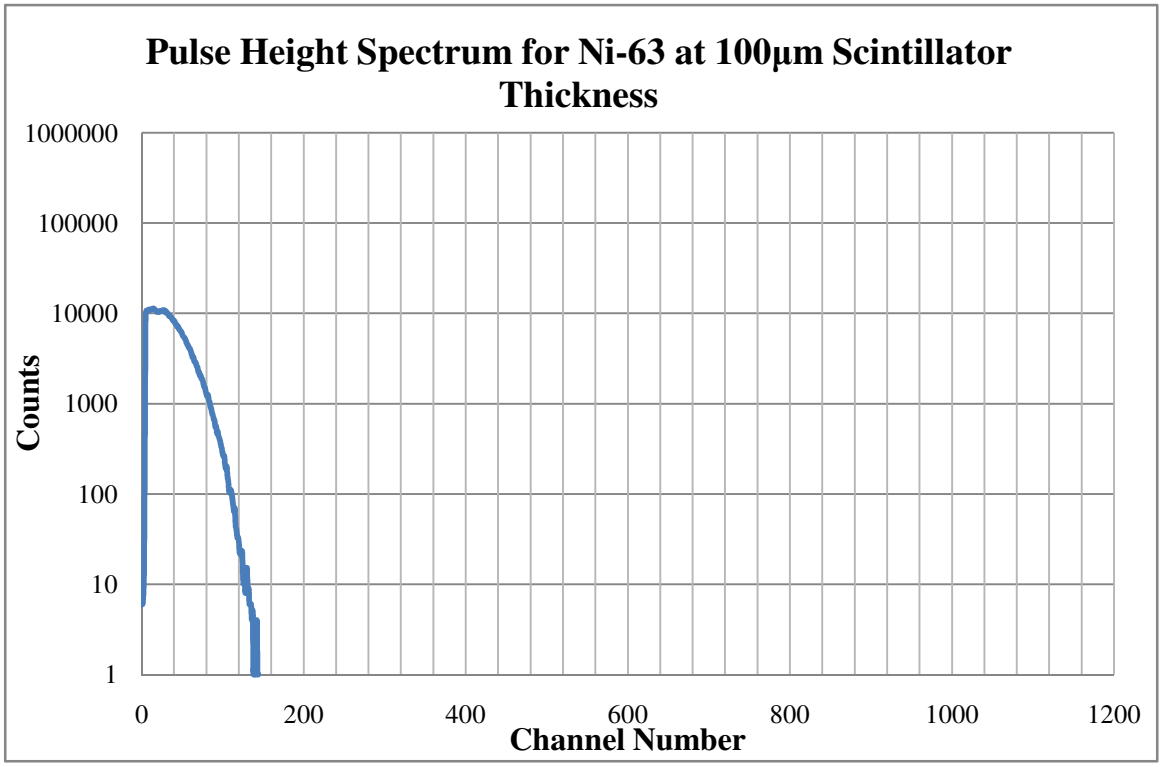

Figure 4.16: Ni-63 at 100µm scintillator thickness

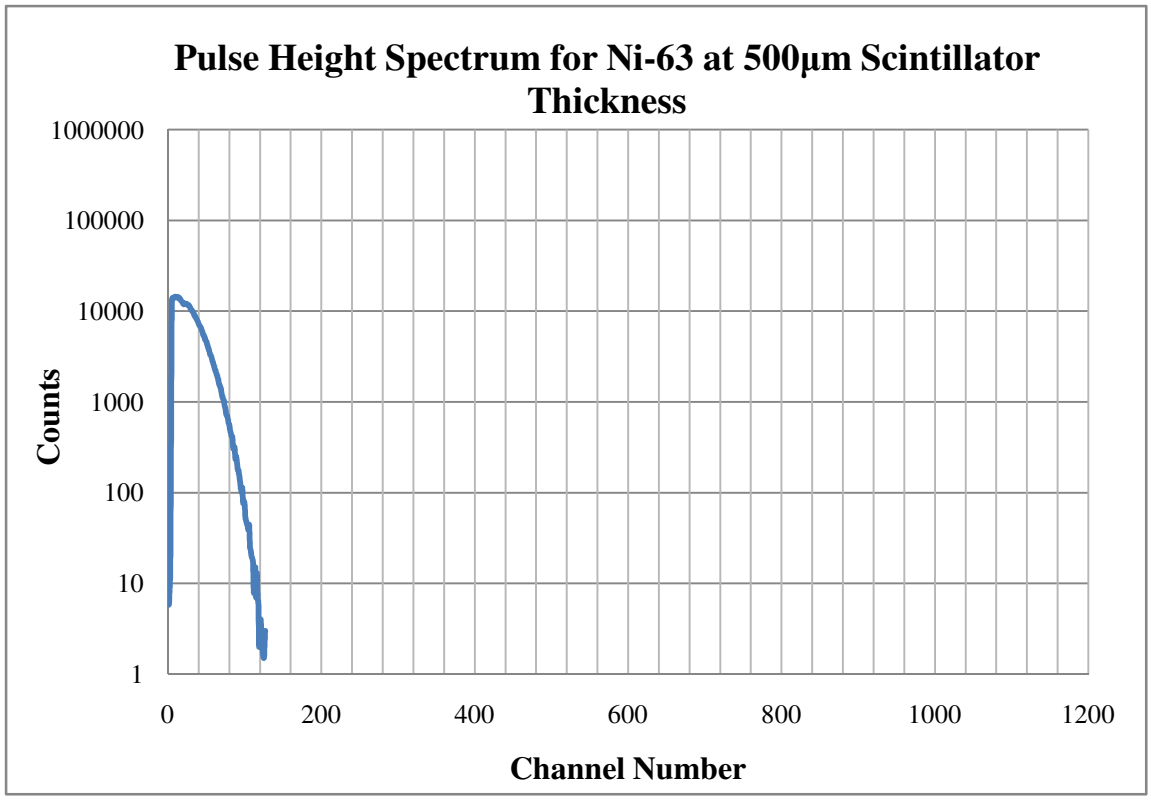

Figure 4.17: Ni-63 at 500µm scintillator thickness

Figures 4.16 and 4.17 shows the distribution of pulse heights for Ni-63 trials and illustrate that there is no significant shift in the pulse heights as the scintillator thickness increases. Taking into account the spectrum shift for high energy gamma photons (Co-60), as well as the consistent channel spread for beta particle emissions from Ni-63, an overlapping of the channels was utilized as a method for obtaining the optimal scintillator thickness. Each scintillator thickness for both sources over the same channel intervals was analyzed by calculating and obtaining a ratio of Ni-63counts to Co-60 counts. The ratio yields the difference for each scintillator thickness between beta particles and high energy photons that result from a given exposure to both sources.

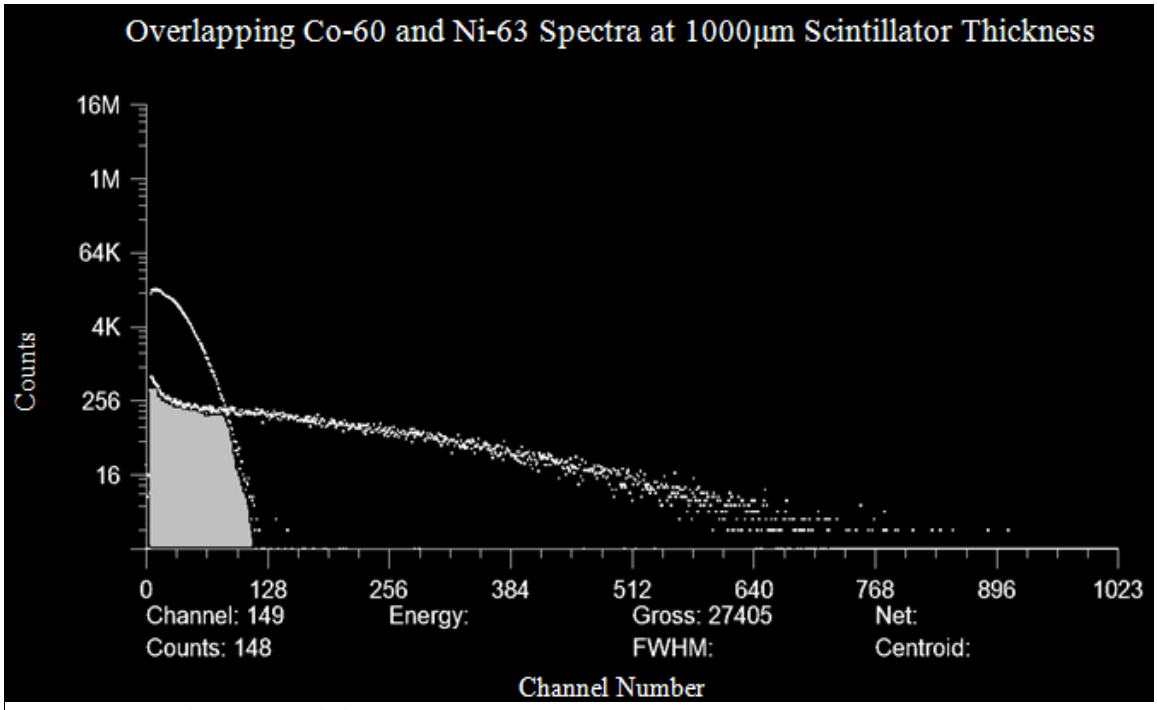

Figure 4.18: Overlap of Co-60 and Ni-63 counts

Figure 4.18, shows the overlap of Ni-63 counts over Co-60 counts at a scintillator thickness of 1000 µm. The scatter plot which ends at approximately channel 128 on the figure indicates the pulses from Ni-63, while the scatter plot which extends over almost the entire spectrum indicates those from Co-60 source. The shaded gray region shows the

region of interest which extends from channel 11 to channel 137 where counts from both source are observed. This methodology was used for each scintillator thickness with the results presented in Table 4.8 and Figure 4.16.

Scintillator Thickness (µm)	Overlapping Channels	Integrated Counts	
		Co-60	**Ni-63**
50	11 – 156	22975	465529
100	11 – 143	21976	488332
250	11 – 135	19157	474018
500	11 – 135	18494	461387
1000	11 – 137	25351	440289
1500	11 – 120	24213	417840
2000	11 - 106	23574	403716

Table 4.8: Co-60 and Ni-63 counts comparison

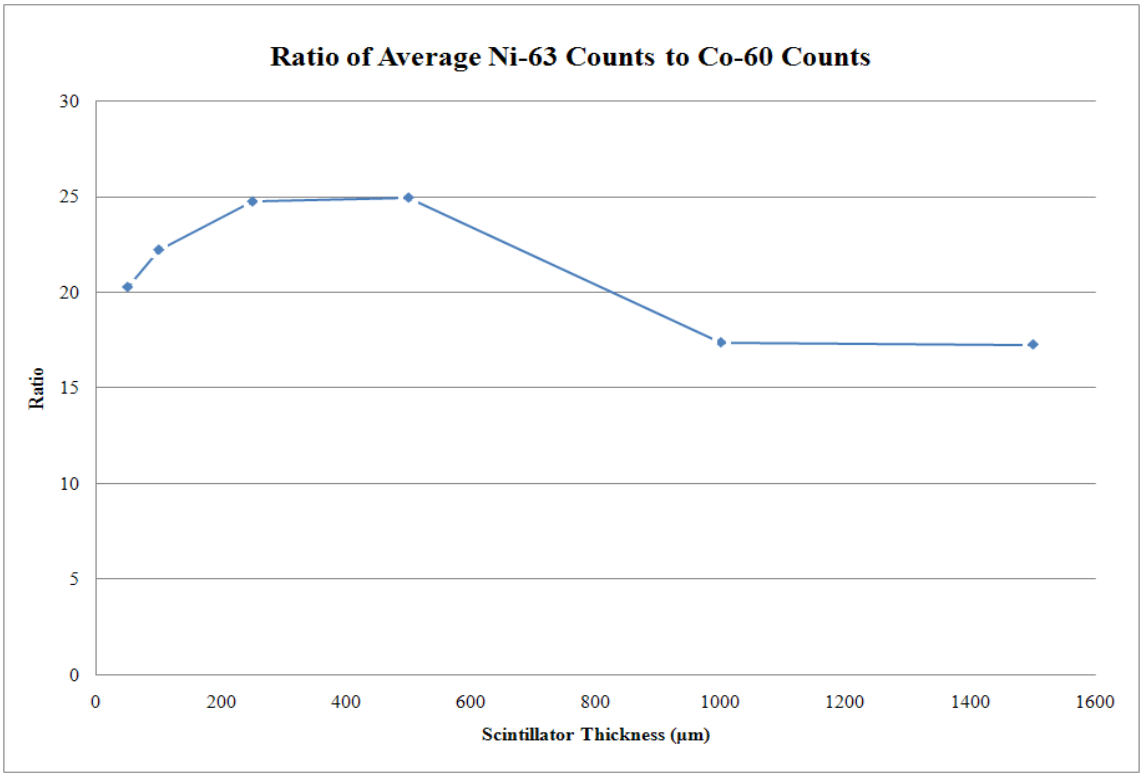

Figure 4.19: Ratio of Average Ni-63 counts to Co-60 counts

From Figure 4.19, a ratio of 25 corresponds to two scintillation thicknesses at 250 μm and 500 μm. The thinner 250 μm scintillator is chosen as the optimal thickness since it is better suited to the experiment as it would provide a greater insensitivity to gamma photons in comparison to the 500 μm scintillator thickness and therefore an overall reduction in count rate. At this optimal scintillator thickness of 250μm, the number of Co-60 counts was found to be 19,157. Measured over a 5 minute period, it equates to a dose rate of 237μGy/hour in plastic. Calculations in acquiring this dose rate can be found in Appendix B. Though this dose rate seems high, it is common in nuclear power plants and represents some of the work environments of nuclear energy workers.

4.5 H-3 Simulation Analysis Results

4.5.1 Calculated Hypothesis for H-3 Simulation

As discussed in Chapter 3, the simulation of H-3 in MCNP4a depends on the range of a beta particle emitted from H-3. The final results of this simulation were compared to the theoretical analysis of the number of tritium beta particles being registered compared to an exposure rate of 237 μGy/hour from high energy photons. The MCNP4A simulations were compared to the calculated theoretical maximum range of H-3 beta particles found through equation 2.4

$$R\left(\frac{mg}{cm^2}\right) = 412(0.0186)^{1.265-0.0954\ln(0.0186)}$$

$$= \frac{0.586mg}{cm^2} * \frac{1g}{1000mg} = \frac{5.86x10^{-4}g}{cm^2} \quad (4.5)$$

Assuming the density of air to be 1.2041 kg/m^3 [28]

$$R = \frac{5.86x10^{-4}g}{cm^2} * \frac{1cm^3}{1.2041x10^{-3}g} = 0.486cm * \frac{10mm}{cm} = 4.86\,mm \quad (4.6)$$

Using the above formula, the maximum range of a tritium beta particle is calculated to be approximately 5mm in air. This range is used as the height of a cylindrical volume of air in which H-3 beta particles are able to reach the scintillator. Given a radius of 6mm (resembling the radius of the scintillation disks) and a height of 5 mm, the volume is calculated as 550 mm[32]. The final step was to determine the number of counts over a 5 minute period. This was calculated via the equation below for a concentration of 1 DAC (300 kBq/m^3) [5]. A Derived Air Concentration (DAC) is the concentration of a radionuclide in air which if a worker were exposed to over a year (2000 working hours) would result in the Annual Limit Intake (ALI) for inhalation. A DAC is based on a breathing rate of 0.02 m^3 of air per minute [5]. The ALI is the activity of a radionuclide which would contribute an effective dose of 20 mSv during a 50 year period after the intake of the radionuclide [32].

The DAC for tritium can also be calculated via Equation 4.7 below:

$$DAC = \frac{ALI}{2000\ working\ hours * \frac{1.2m^3}{hr} * 1.5}$$

$$= \frac{1x10^9}{2000hrs * \frac{1.2m^3}{hr} * 1.5} = 3x10^5\ Bq/m^3 \qquad (4.7)$$

The factor of 1.5 allows for skin absorption [5].

Detectable activity can be calculated to be:

$$A_D = V * DAC = 549.65mm^3 * \frac{1.0x10^{-9}m^3}{1mm^3} * \frac{300kBq}{m^3} * \frac{1000Bq}{1kBq} = 0.164896\ Bq \qquad (4.8)$$

Since the definition of Becquerel is one disintegration per second, and each disintegration results in a count, the count rate from this activity over a 5 minute period can be calculated as:

$$C.R = \frac{0.164896 counts}{sec} * \frac{60 sec}{min} * 5 min = 49.5 counts \quad (4.9)$$

This expected number of counts represents a situation where all the H-3 beta particles travel towards the PMT. A realistic assumption would include dividing the counts in half to account for the fact that the beta particles are emitted isotropically and on average only half of the emitted betas will be travelling towards the PMT. This assumption is based on the isotropic emission being a 4π distribution while the simulated geometry would have a 2π direction thus simulating a planar source. Following this assumption, the resulting counts would yield approximately 24.7 counts over a 5 minute period.

4.5.2 Simulated Results for the Range of Beta Particles Emitted from Tritium

Two scenarios were attempted in MCNP4a which featured a vacuum and air medium respectively with particles in both scenarios being emitted isotropically. While the initial setup was shown in Chapter 3, a more accurate visual representation can be found using VISED. VISED is a visual editor created for the MCNP code and is helpful when analyzing the setup.

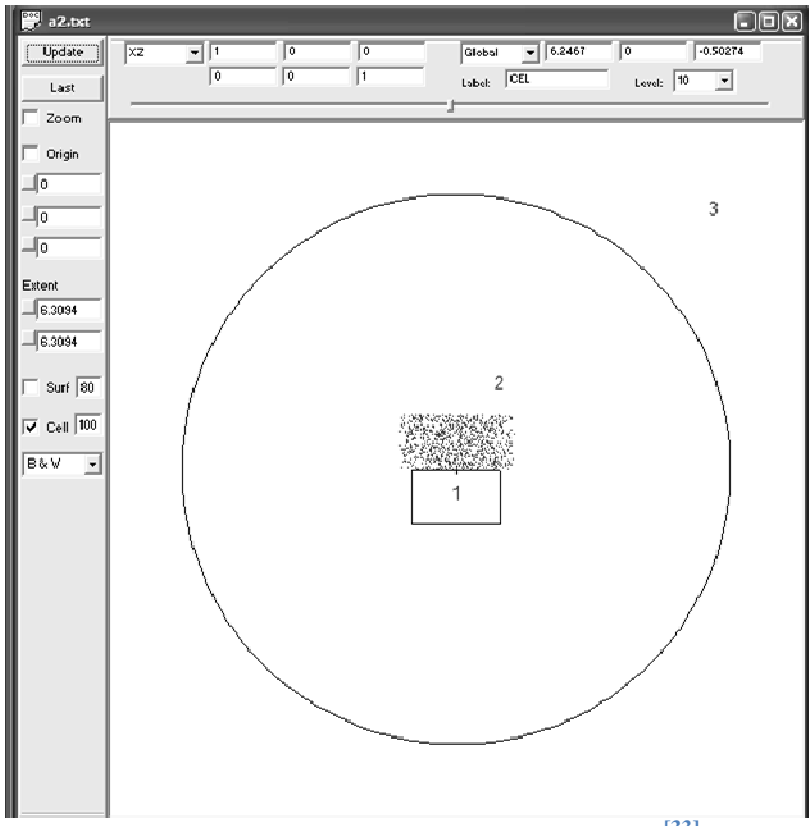

Figure 4:20: VISED setup of MCNP Results [33]

Figure 4.20 shows a MCNP 4a setup in VISED where the volume source is defined in a spherical universe which sits on top of a PMT. The code when run, scores the number of beta particles that cross the top surface of the PMT, which in turn represents the scintillator surface. The first scenario leaves the universe in a vacuum state and the second fills the spherical universe with air. The codes for both these scenarios may be found in Appendix A with supplementary comments for each scenario. The basic code in MCNP is not difficult to use depending on the complexities of the design simulation and the understanding of the code structure. A brief description will be provided here.

An MCNP input file starts with a title card, followed by cell cards which are made up and followed by surface cards which are then followed by data cards. The cell and surface cards contain geometrical information of the setup, while the data cards contain

source information cards as well as tally cards which inform the program of how the source is set up along with the type of emission it produces. Each set of cards are separated with a blank line in order for the program to differentiate between each set. Comments are added into the code via symbols such as '$' or 'c'. The source cards are perhaps the most difficult to understand and are symbolized with an 'sdef', meaning source definition. 'Pos' refers to position and is a reference point for the sampling position. 'Axs' refers to axis and is a reference vector for 'ext' and 'rad'. 'Rad' refers to radius and is the radius dimensions of the source. 'Ext' refers to the distance from the position along a cell case ('axs'). The 'ext' can also be symbolized as the height of a cylindrical source [39]. In the code above, the source cards include 'ext'=d1 while 'rad'=d2. Each'd' includes a source intensity card (si) and a source probability card (sp). The source intensity card defines the co-ordinates for the radius of the source, while the source probability cards define the distribution of the source. In the case above, -21 0, refers to an even distribution of the source in the cylindrical volume [25]. These source definition cards are followed by the tally cards, which record the number of particles crossing a particular surface as well as the current tally, which is the number of histories the program runs. The input file ends with these tallies and outputs a ratio of the number of particle to cross the specified boundary to the total number of particles present in the created universe [34,24].

4.5.2.1 Vacuum Scenario

The tally for the vacuum scenario yielded a surface tally of 0.15893, the ratio of the number of beta particles that crossed the PMT surface to the total number of beta particles emitted. In order to obtain the number of counts over a 5 minute period, the

ratio obtained from the MCNP run is now used. A volumetric H-3 beta source was simulated with a diameter of 21 mm. The photocathode diameter of the PMT was 16 mm and an extra 5mm was added in order to ensure the source was a bit larger than the PMT diameter, thus allowing for beta particles to reach the PMT from a solid angle of 2π. Using this radius, the volume of the source was found and multiplied by the surface tally and the DAC for tritium to calculate the activity over a 5 minute period for 100,000 histories in a vacuum scenario. These 100,000 histories serve as a probabilistic assessment of the accuracy of the output. As the histories for each program is increased, the result provides a better approximation to realistic scenarios. These histories are not taken into consideration for calculations as their purpose is to provide the most precise output as possible. Therefore the calculations using the ratio obtained from the simulation were as follows:

Radius of source:

$$16mm + 5mm = 21mm * \frac{1cm}{10mm} = \frac{2.1cm}{2} = 1.05\ cm \tag{4.10}$$

Volume of uniform H-3 beta source:

$$= \pi r^2 H = \pi(0.0106)^2(0.01) = 3.53x10^{-6}\ m^3 \tag{4.11}$$

Activity:

$$A = \frac{300kBq}{m^3} * \frac{1000Bq}{kBq} * 3.53x10^{-6}m^3 * 0.15893 = 0.1683\ Bq \tag{4.12}$$

Number of counts achieved over 5 minutes:

$$C = \frac{0.1683 dis}{sec} * \frac{60 sec}{min} * 5 min = 50.5\ counts \quad (4.13)$$

Therefore, the simulated activity for the vacuum scenario yielded 50.5 counts over a 5 minute period.

4.5.2.1Air Medium

The code for the spherical universe filled with air can found in Appendix A and accounts for this difference in the material cards of the code. This scenario was run with the spherical universe filled with air which simulates tritium beta particles in air. Air was referenced as a combination of the following constituent elements:

Element	Yield (Weight Fraction) (%)	Associated MCNP code
Hydrogen	1.18	1000
Nitrogen	77.08	7000
Oxygen	21.28	8000
Argon	0.46	18000

Table 4.9: Constituent Elements of Air [28]

The associated density of air was assumed as 1.24×10^{-3} g/cm^3 [28]

This run for beta particles placed in a medium of air resulted in the tally through the plastic scintillator of 0.06728. Using this ratio, the volume and DAC from the calculations carried out in scenario one, the count rate over a 5 minute period for 100,000 histories was calculated as follows:

Activity:

$$A = \frac{3.0x10^5 Bq}{m^3} * 3.53x10^{-6} m^3 * 0.06728 = \frac{0.07125 dis}{sec} \quad (4.14)$$

Number of counts achieved over 5 minutes:

$$C = \frac{0.07125 dis}{sec} * \frac{60 sec}{min} * 5 min = 21.4\ counts \quad (4.15)$$

The simulated activity for the air medium scenario thus yielded 21.4 counts over a 5 minute period. This result can now be compared to the calculated hypothesis that accounted for beta particles being emitted isotropically in an air medium with a yield of 24.7 counts over a 5 minute period.

$$Deviation = \frac{|calculated - simulated|}{simulated} * 100 = \frac{|24.7 - 21.4|}{21.4} * 100 = 15.7\% \quad (4.16)$$

The simulated value deviates from the calculated value by 15%, possibly due to the scatter that may have occurred when air is present. The assumption that only half the beta particles reach the detector was an overestimation as the MCNP version shows that less than half reach the scintillator.

Chapter 5: Future Developments and Related Studies

Conclusions drawn from Chapter 4 established the count rate over a 5 minute period from tritium to be minimal and not enough to be discernable in a high energy gamma background such as Co-60. The development of a personal tritium monitor may not be possible at present. The concepts developed during this research may however be useful to develop noble gas monitors or contribute to the development of stack monitors and warranty further investigation.

5.1 Stack Monitors

Stack monitors detect radioactive particulates that are vented from different rooms inside nuclear facilities. They are also used to sample air being vented from the facilities vent stack to the environment. These radioactive particulates may include iodine, noble gases, and tritium. The detection of these particulates serves to ensure compliance with established derived emission limits (DEL) approved by the Atomic Energy Control Board. The monitors ensure that the release to the environment does not cause members of the public to receive an effective dose greater than 0.1mSv/year. Due to this reason monitors are required to have central readouts and accessible alarms panels to allow an evaluation of environmental conditions following an accident [35,36].

Other radionuclides involved in a release could include Xenon, Krypton and Argon. Some of these radionuclides emit both, beta and gamma radiation, while others emit only gamma radiation. Among the beta emitters are radionuclides such as Xe-135, Xe-133, Kr-88 and Ar-41. Calculations of the activity over a 5 minute period carried out for tritium during this research were also repeated for other beta-emitter radionuclides to

determine the prospects of plastic scintillators for stack monitoring. Using a 1 DAC limit (the same as for tritium), the nuclear regulatory commission was used to obtain the DAC amounts for each radionuclide.

Radionuclide	Max Energy(MeV)	Probability	DAC ($\mu Ci/cm^3$)
Xe-135	0.909	0.961	$1x10^{-5}$
Xe-133	0.346	0.993	$1x10^{-4}$
Kr-88	0.521	0.67	$1x10^{-6}$
Ar-41	1.198	0.99	$1x10^{-6}$

Table 5.1: Table of radionuclides detected by stack monitoring [37]

Using the energy of each radionuclide, the range was determined using the range equation for beta particles mentioned in chapter 2 (Equation 2.5). As was done with tritium, the range was used as the height of a cylinder simulating the farthest distance a particle from the detector would have to travel to reach the detector. This volume of air in which the beta particles exist may be multiplied by the DAC to obtain the number of counts as was done in Chapter 4 for the analytical calculations of tritium. The results over a 5 minute period are shown in table 5.2

Radionuclide	**Range (mm)**	**Volume of Air Surrounding the Detector (m^3)**	**DAC(Bq/m^3)**	**Counts (over 5 minutes)**
Xe-135	$3.03x10^{3}$	$3.42x10^{-4}$	$3.7x10^{5}$	37,962
Xe-133	$8.04x10^{2}$	$9.09x10^{-5}$	$3.7x10^{6}$	100,899
Kr-88	$1.44x10^{3}$	$1.62x10^{-4}$	$7.4x10^{4}$	3596.4
Ar-41	$4.28x10^{3}$	$4.84x10^{-4}$	$1.11x10^{5}$	16,117.2

Table 5.2: Range of Radionuclides used to calculate the volume of air surrounding the detector. Used with the DAC to obtain the counts over a 5 minute interval.

From table 5.2, it can be noted that most of the counts are not sufficiently high enough to differentiate between the betas coming from its respective radionuclide as compared to 19,000 counts from the Co-60 source delivering a dose rate of 237 μGy/hr. The exception to these radionuclides is Xe-133 which yields approximately 100,000 counts over a 5 minute period. Further investigation may be needed to determine the feasibility of using this research to develop a stack monitor for specific radionuclides.

Presently, gas-flow proportional counters are used to monitor stack gases at CANDU plants, but feedback and the presence of different noble gases limits the attainable compensation with these monitors. Presently, gas-flow proportional counters are the most suited instrument for monitoring stack effluent from CANDU facilities as it provides good gamma and noble gas compensation as well as high tritium sensitivity [5].

5.2 Analysis of Other Investigations

The optimization of scintillator thickness for plastic scintillators for low energy beta particles in high energy gamma backgrounds is being pursued by other companies and research laboratories as well.

One of these companies is the Canberra Corporation which supported research done by a UOIT masters graduate with the objective of enhancing one of their products, the "Argos full body monitor". The system produces low detection efficiency and requires long counting periods. The objective of the thesis included identifying the optimal plastic scintillator thickness for better efficiency for the unit in order to improve beta detection. The experimental findings utilized a 150μm thickness of EJ-212 series plastic scintillator and the results showed a low detection efficiency of about 6% for Carbon-14(156 keV), a beta emitter, and about 24% for Chlorine-36 (709 keV). The

study then investigated different trials via an MCNP simulation using plastic scintillator thicknesses of 150 μm to 600 μm with the purpose of optimizing the thickness of the scintillation material required to be insensitive to gamma radiation while simultaneously incorporating maximum beta detection. The main findings via experimental and simulation setups concluded a thickness between 300 μm and 500 μm. This optimal scintillator thickness was found applicable for high efficiency beta detection in the presence of low energy gamma rays [14].

This research is significant because it can also provide a comparison to the optimal scintillator thickness found for the current work. The conclusion from the previous thesis suggested a lower limit of 300 μm which is similar to the results obtained during the investigation of the optimal scintillator thickness between Ni-63, a low energy beta source and Co-60, a high energy gamma source to be 250 μm. Although the two results are similar, the investigations differ with respect to the energies of each type of radiation. While the previous thesis investigated the optimal thickness of high energy beta particles to low energy gamma rays, this thesis investigated the optimal thickness for high energy gamma rays and low energy beta particles. The achievement of similar results from both these investigations can be explained by analyzing the energy deposition from each source. The amount of energy deposited in a medium depends on the stopping power and the thickness of the medium. Equation 5.1 shows this relationship as:

$$\Delta E = \frac{de}{dx} * \Delta x \tag{5.1}$$

Where Δx = Change of thickness in medium

de/dx = Stopping power

Source	Average Energy	de/dx (MeV•cm^2/g)
Ni-63	17.5keV	14.6
C-14	50keV	6.2
Cl-36	200keV	2.8

Table 5.3: Stopping Powers for Various Beta Sources [39]

As table 5.3 shows, the stopping power of Ni-63 is greater than Cl-36 which means for Ni-63, a smaller scintillator thickness would be required as compared to Cl-36 in order to deposit the same energy from each beta particle interactions with the scintillator. When comparing these beta particles being detected in a high energy gamma background, it is noted that Am-241 which is a lower energy gamma source produces approximately the same pulse height distribution as scintillator thickness increases. Therefore, the dominating factor when determining the optimal scintillator thickness with mixed fields of high energy beta particles and low energy gamma photons is the energy of the beta particles. In the case of low energy beta particles compared to high energy gamma photons, the gamma pulse height spectrum needs to be considered. Obtaining similar results for beta-gamma mixed field dosimetry is encouraging however a closer analysis is warranted in order to understand the exact mechanism resulting in the behavior observed for each investigation.

Chapter 6: Conclusion

The purpose of this work was to study the behavior of plastic scintillators to gamma photons and beta particles in order to assess the feasibility of building a personal tritium monitor capable of operating in a high energy gamma background. This research is important because a personal tritium monitor does not exist presently and using plastic scintillators as the detecting medium has significant advantages over current detectors.

Adhering to these advantages the first part of this investigation involved analyzing the response of plastic scintillators to four different gamma sources, namely, Iron-55, Americium-241, Cesium-137 and Cobalt-60. The experimental data showed a linear relationship between the gamma ray sensitivities of plastic scintillators and their thickness. The attenuation of gamma rays as a function of energy supported the experimental data. As the attenuation coefficient decreased, fewer photons were stopped for a given scintillator thickness and vice versa. This was the case with the Am-241 and Co-60 sources. The Cs-137 source initially resulted in an increased count rate due to the emission of beta particles from the source which were stopped by a 0.128 mm copper disk. The placement of the copper disk yielded results which agreed with the hypothesis. The hypothesis was based on the attenuation coefficients of the respective sources. Fe-55 followed this increasing linear trend to a thickness of 1000 μm, with this thickness being the saturation point for the gamma emissions from the source. Calculations proved that at this thickness approximately 90% of photon emissions from the source had been attenuated and any additional thickness would only serve as an obstruction, limiting the number of light photons reaching the PMT.

This result was shared when observing the effects of beta particles emitted by the Nickel-63 source which was used to analyze the response of plastic scintillators to beta particles. Scintillator placement and the application of optical grease produced informative and consistent results. These two factors would have to be taken into consideration when building a beta detector with the use of plastic scintillators. The results produced were in agreement with the hypothesis and calculated values. The graph showed an increase in the number of counts registered by the PMT up to a scintillator thickness of 50μm. This is the closest measurement to the theoretical value of 63μm calculated as the thickness needed to stop most beta emissions from the source. The number of counts decreased gradually as additional scintillation material was added. This was due to the number of light photons from the scintillator being obstructed by the extra material thus decreasing the total integrated counts.

After assessing the behavior of photons and beta particles to plastic scintillators, the optimal scintillator thickness was found to be 250 μm. This thickness discriminated Co-60 gamma photons while being sensitive to Ni-63 beta particles by yielding a ratio of 25 when comparing the integrated counts over the same channel numbers of the two sources. This was determined by comparing the highest energy gamma source to the low energy beta source over the same number of pulse-height channels. At this thickness, the high energy photon background would result in approximately 19,000 counts being registered by the detector for a dose of 237 μGy/ hour over a 5 minute period, while Ni-63 would contribute approximately 474,000 counts at the same thickness over the same time period. For the same photon dose rate, the number of H-3 betas detected would have to be greater than the 19,000 counts obtained from the Co-60 source for the tritium signal

to be discernable over the same interval period of 5 minutes. An MCNP simulation was constructed to model the interaction of tritium beta particles with the detector system which was the final part to this investigation.

Using a tritium concentration of 1 DAC produced results which were compared to analytical calculations using the same concentration over a 5 minute interval. The comparison of these counts to 19,000 counts obtained from the Co-60 was insufficient to build a personal tritium monitor. The simulated scenario yielded 21 counts as compared to the calculated scenario which yielded 24 counts. This deviation is small enough to justify the calculations for such problems as being an accurate method to obtain the required result. From the concluding results however, it was determined that a tritium monitor capable of operating in a high energy gamma background is not possible due to sensitivity of the detector and the low count rate that would be obtained from the tritium. The deviation of 15% between the analytical calculations and the simulated counts also confirmed the accuracy of the calculations which can be applied to other radionuclides in order to determine a different use for the research done for this investigation.

One of these uses may be applied towards detecting low energy gamma radiation such as Fe-55 in a high energy gamma background. The technique of choosing the optimal scintillator thickness developed through this research may be used for other radionuclides to differentiate between low energy beta radiation or low energy gamma radiation, and high energy gamma radiation. Overall, the method of optimization of plastic scintillators established in this work agrees with results obtained by others using simulation, analytical, and experimental work. Plastic scintillators are ideal in such

situations due to the distinct advantages mentioned earlier which makes them important in the development of instrumentation in the field of health physics.

Appendix A: MCNP Code for Tritium Simulations

```
c Thesis Project: To determine the number of counts that would reach a simulated PMT from a volumetric H-3 source in a vacuum scenario
1   0    -1 -2 3          $This volume card defines the inside of the PMT via the first 3surface cards
2   0     #1 #3           $This volume card defines the outside of the PMT but inside the universe which is where the source will be placed
3   0     4               $This volume card defines the outside of the universe which is the graveyard region

c ************************
1    cz 0.8               $This surface card creates a infinite cylinder in the z-axis around z=0.8
2    pz 0                 $This surface card creates a plane that cuts the z-axis at z=0 to form the top of the cylinder/PMT
3    pz -1                $This surface card creates a plane that cuts the z-axis at z=-1 to form the bottom of the cylinder/PMT
4    so 5                 $This surface card creates a sphere which defines the universe and starts at the origin(0,0,0) with radius 5

c ***************************************
mode E                                          $This data card defines the specific particles which in this case are electrons
imp:e 1 1 0                                     $This data card defines the importance of the cells
sdef pos=0 0 0 axs=0 0 1 par=3 rad=d1 erg=0.018601 ext=d2   $The date cards defines the parameters of the source which are beta particles/electrons
                                                $which have an energy of 18.6keV, placed at the origin(0,0,0)with in the z axis, with the
                                                $radius and distance from the position along the z-axis being specially defined (d1,d2).
                                                $Each 'd' has a corresponding SI(source intensity) and SP(source probability).
SI1 0 1.05                                      $This source intensity card defines the radius of the source which as 1.05cm
SP1 -21 1                                       $This source probability card defines the radius to be an evenly distributed probability
SI2 0 1                                         $This source intensity card defines the height of the volume source to be 1cm
SP2 -21 0                                       $This source probability card defines the height of the source to have an evenly distributed probability
F1:e 2                                          $This data card specifies a tally through surface 2 (top of PMT) which counts the number of particles
                                                $that cross the top of the PMT
nps 100000                                      $This data specifies the number of histories which in this case is a hundred thousand particles
```

```
c Thesis Project:To determine the number of counts that would reach a simulated PMT from a volumetric H-3 source when the universe is air filled
1   1   -0.00124   -1 -2 3        $Card defining inside of the PMT which is filled with material 1 that has an atom density of 1.24g/cm^3
2   1   -0.00124   #1 #3          $Card defining the outside of the PMT & inside the universe which is filled with material 1 and has an atom density of 1.24g/cm^3
3   0              4              $Card defining the outside of the universe which is the graveyard region that has no material

c ****************************************
1    cz 0.8                       $This surface card creates a infinite cylinder in the z-axis around z=0.8
2    pz 0                         $This surface card creates a plane that cuts the z-axis at z=0 to form the top of the cylinder/PMT
3    pz -1                        $This surface card creates a plane that cuts the z-axis at z=-1 to form the bottom of the cylinder/PMT
4    so 5                         $This surface card creates a sphere which defines the universe and starts at the origin(0,0,0) with radius 5

c ****************************************
mode E                                                  $This data card defines the specific particles which in this case are electrons
imp:e 1 1 0                                             $This data card defines the importance of the cells
M1   1000   -0.0118                                     $The next 4 data card defines material 1 which consists of hydrogen with weight fraction of 1.18%
     7000   -0.7708                                     $Nitrogen with weight fraction 77.08%
     8000   -0.2128                                     $Oxygen with weight fraction 21.8%
     18000   -0.0046                                    $and Argon with weight fraction 0.46%
sdef pos=0 0 0 axs=0 0 1 par=3 rad=d1 erg=0.018601 ext=d2   $The data cards defines the parameters of the source which are beta particles/electrons which
                                                        $have an energy of 18.6keV, placed at the origin(0,0,0)with in the z axis, with the radius and
                                                        $distance from the position along the z-axis being specially defined (d1,d2). Each 'd' has a
                                                        $corresponding SI(source intensity) and SP(source probability).
SI1 0 1.05                                              $This source intensity card defines the radius of the source which as 1.05cm
SP1 -21 1                                               $This source probability card defines the radius to be an evenly distributed probability
SI2 0 1                                                 $This source intensity card defines the height of the volume source to be 1cm
SP2 -21 0                                               $This source probability card defines the height of the source to have an evenly distributed $probability
F1:e 2                                                  $This data card specifies a tally through surface 2 (top of PMT) which counts the number of particles
                                                        $that cross the top of the PMT
nps 100000                                              $This data specifies the number of histories which in this case is a hundred thousand particles
```

Appendix B: Exposure Rate of Co-60 Gamma Source

Calculating the exposure rate of the Co-60 source used is essential since a personal detection monitor depends on the exposure rate of the environment. To calculate the exposure rate of the Co-60 source used, the activity must be known. The total activity emitted by the source is calculated from the following equations:

$$A(t) = A_o e^{-\lambda(t)}$$ [12]

Where

$$\lambda = \frac{\ln 2}{T_{\frac{1}{2}}}$$

And

A_o = 1 μCi

$T_{1/2}$= 5.27 yrs

t= 5.66 yrs

The activity equation above can be explained due to the decay of a source being an exponential trend. The half life of a source ($T_{1/2}$) is the amount of time that it takes an isotope to decay by exactly half of its original activity [6]. This equation is a standard equation used to find the activity at the current time symbolized by the variable A(t), with A_o symbolizing the activity of the source when created.

Therefore, it is used to determine the initial activity of the Co-60 source.

$$A(t) = 1x10^{-6}Ci * \left(e^{-\frac{ln2}{5.27}*5.66}\right) = 4.75x10^{-7}Ci$$

Converting to S.I units:

$$A(t) = 4.75x10^{-7}Ci * \frac{3.7x10^{10}Bq}{Ci} * \frac{MBq}{1x10^{6}Bq} = 17.6x10^{-3}MBq$$

Using the above solution, the exposure rate in air can be calculated with the known specific gamma-ray constant of Co-60. The gamma-radiation exposure rate from a point source of unit activity at unit distance is termed the specific gamma ray constant and is measured in units of coulombs per kilogram per hour at 1m from a 1-MBq point source[1,12]. Specific gamma ray emissions can be theoretically calculated when the exposure is measured in roentgens and the activity is known in curies.

$$\Gamma = 0.5 \sum_i f_i * E_i \frac{\left(\frac{C}{kg}\right)m^2}{MBq \bullet h} \quad [12]$$

Where f_i = fraction of the transformations that yield a photons whose energy is E_i

The specific gamma-ray constant for Co-60 was found to be $9.19x10^{-9}\frac{X \bullet m^2}{MBq \bullet h}$.[12]

Therefore using the activity of Co-60 found earlier in conjunction with the specific gamma ray constant of Co-60, the exposure rate in Air at 1m from Co-60 is found as:

Exposure at 1m= $\frac{9.19x10^{-9}X}{MBq*hr} * 17.6x10^{-3}MBq = \frac{1.61x10^{-10}X}{hr}$

Where X = C/kg

Once this exposure rate at 1 meter is found, applying the inverse square law will yield the exposure rate at a specific distance (5mm for this experimental purpose and the distance

from the source to the scintillator). The inverse square law is mathematically represented below and states that as the distance between a source and a target is doubled, the intensity is reduced four fold.

$$\frac{I_1}{I_2} = \frac{{X_2}^2}{{X_1}^2} \quad [29]$$

Thus $I_1 = 1.61\text{x}10^{-10}$ X/hr

X_1=1m

X_2= $5\text{x}10^{-3}$ m

$$I_2 = \frac{I_1}{\frac{{X_2}^2}{{X_1}^2}} = \frac{1.61x10^{-10}}{\frac{(5x10^{-3})^2}{1^2}} = \frac{6.44x10^{-6}X}{hr}$$

Therefore, the exposure rate in air at a distance of 5mm was found to be $6.44\text{x}10^{-6}$ X/hr. In order to convert the exposure rate in air to the dose rate in plastic, the mass energy absorption coefficient needs to be known for plastic and air. The average energy expended in air per ion pair formed (W_{air}) also needs to be known. It is the initial kinetic energy of a charged particle (E_k) divided by the mean number of ion pairs formed from that charged particle as it completely dissipates its energy in air.

$$\frac{W_{air}}{e} = \frac{E}{N} \quad [30]$$

Where E= total energy deposited in air volume

N=total number of ion pairs produced in the air volume

The current best estimate for the average value of W_{air} is $33.97\ \frac{eV}{ion\ pair}$ or $33.97x10^{-19}\ \frac{J}{ion\ pair}$. [30]

$$\frac{W_{air}}{e} = \frac{33.97\left(\frac{ev}{ion\ pair}\right) * \frac{1.602x10^{-19}J}{ev}}{\frac{1.602x10^{-19}C}{ion\ pair}} = \frac{33.97J}{C}$$

Multiplying this value by the ratio of the mass energy absorption coefficient of plastic to air and the exposure rate found in air, yields the dose rate in plastic. The mass attenuation coefficient (μ_{en}/ρ) for the average energy of Co-60 through a medium of air and plastic was found to be the following:

$$Average\ Energy\ of\ Co-60 = \frac{1.332MeV + 1.172MeV}{2} = 1.25\ MeV$$

For 1.25MeV: μ_{en}/ρ for plastic scintillators: $2.894x10^{-2}\ cm^2/g$ [31]

For 1.25MeV: μ_{en}/ρ for air: $2.666x10^{-2}\ cm^2/g$ [31]

Dose Rate in Plastic:

$$D_{plastic} = X_{air} * (\frac{W}{e})_{air} * (\frac{\mu_{en}}{\rho})_{air}^{plastic} \quad [30]$$

Where

X_{air}= exposure rate in air = $6.44x10^{-6}\ \frac{x}{hr} = 6.44x10^{-6}\ \frac{C}{kg \cdot hr}$

$(\frac{W}{e})_{air} = charge\ per\ unit\ mass\ of\ air = 33.97\ \frac{\mathrm{J}}{\mathrm{C}}$

$\left(\frac{\mu_{en}}{\rho}\right)^{plastic} = \frac{2.894*10^{-2}cm^2}{g}$

$\left(\frac{\mu_{en}}{\rho}\right)^{air} = \frac{2.666 * 10^{-2}cm^2}{g}$

$$D_{plastic} = \frac{6.44x10^{-6}C}{kg \bullet hr} * \left(\frac{33.97J}{C}\right) * \left(\frac{\frac{2.894x10^{-2}cm^2}{g}}{\frac{2.666x10^{-2}cm^2}{g}}\right) = \frac{2.37x10^{-4}Gy}{hr}$$

$$= \frac{2.37x10^{2}\mu Gy}{hr}$$

Therefore, the dose rate measured over a 5 minute period from Co-60 is found to be 237μGy/hour in plastic.

References

1. Cooper, John R., Keith Randle, and Ranjeet S. Sokhi. *Radioactive Releases in the Environment: Impact and Assessment*. Chichester, West Sussex, England: J. Wiley, 2003. Print.

2. Evans, R. D. *The Atomic Nucleus*. McGraw-Hill, 1955. Print.

3. "Annual Limit Intakes (ALI)." *Université D'Ottawa - University of Ottawa*. University of Ottawa. Web. <http://www.uottawa.ca/services/ehss/radali.htm>.

4. Knoll, Glenn F. *Radiation Detection and Measurement*. New York: Wiley, 2000. Print.

5. Wood, M. J., and R. A. Surrette. Real Time Tritium-in-Air Monitors for CANDU Facilities. Tech. no. COG-93-427. Chalk River: AECL, 1994. Print.

6. Hall, Eric J., and Amato J. Giaccia. *Radiobiology for the Radiologist*. Philadelphia: Lippincott Williams & Wilkins, 200. Print.

7. RadDecay. Computer software. Vers. 3.6. Web.

8. Thompson, Patsy. *Darlington New Build Project Joint Review Panel*. Rep. no. 2.01. Canadian Nuclear Safety Comission, 29 Mar. 2011. Web. <http://www.ceaa.gc.ca/050/documents/49178/49178F.pdf>.

9. Cowper, G., and R. V. Osborne. Measurement of Tritium in Air in the Presence of Gamma Radiation. Tech. 45th ed. Vol. R1. Rome: International Radiation Protection Association, 1966. Print

10. Shu, W. M., M. Matsuyama, T. Suzuki, and M. F. Nishi. "Characteristics of a Promising Tritium Process Monitor Detecting Bremsstrahlung X-rays." Nuclear Instruments and Methods in Physics Research (2003). Print.

11. Vikis, A. C. "Recent Progress in Health Physics R&D." 2010 ISOE North American ALARA Symposium/EPRI Radiation Protection Conference. Florida, Fort Lauderdale. Speech.

12. Cember, Herman. Introduction to Health Physics. 3rd ed. New York: McGraw-Hill, Health Professions Division, 1996. Print.

13. Larson, Brian. "Attenuation Coefficient." *NDT Resource Center*. Iowa State University, 2001. Web. <http://www.ndt-ed.org/EducationResources/CommunityCollege/Radiography/Physics/attenuationCoef.htm>.

14. Pourtangestani, Khadijeh K. *Optimization of Plastic Scintillator Thickness for Online Beta Detection in Mixed Fields*. MaSc Thesis. University of Ontario Institute of Technology, 2010.*UOIT*.

15. Miramonti, Lino. "A Plastic Scintillator Detector for Beta Particles." *Pergamon: Radiation Measurements* (2002). Print.

16. Basile, Louis J. "*Progress In Plastic Scintillators*". *Argonne National Laboratory ,Argonne, Illiniois*. Liquid Scintillation Counting International. Web. <http://lsc-international.org/conf/pfiles/lsc1960_161.pdf>.

17. *Hamamatsu - Metal Package Photomultiplier Tube R7400U Series*. Rep. Japan: Hamamatsu, 2004. Print

18. *University of Chicago*. Rep. Burle Technologies, 31 Oct. 2008. Web. <http://psec.uchicago.edu/links/Photomultiplier_Handbook.pdf>.

19. "EJ-212." *Eljen Technolgy*. Sweetwater,Texas,1997. Web. <http://www.eljentechnology.com/index.php?option=com_content&view=article&id=94%3Aej-550&catid=35&Itemid=60>.

20. Saint-Gobain Crystals. *Scintillation Products*. Hlram: Saint-Gobain Crystals, 2001. Print.

21. "EJ-550 & EJ-552." *Eljen Technolgy*. Sweetwater,Texas,1997. Web. <http://www.eljentechnology.com/index.php?option=com_content&view=article&id=64%3Aej-212&catid=31&Itemid=34>.

22. *Integrated Computer Software*. Computer software. *Http://www.spectrumtechniques.com*. Spectrum Techniques, Inc., Feb. 2005. Web.

23. Shultis, J. K., and R. E. Faw. *An MCNP Primer*. Rep. Manhattan: Kansas State University, 2004. Print.

24. *Chapter 1: MCNP and the Monte Carlo Method*. Rep. 2000. Print. Primer.

25. X-5 Monte Carlo Team. *MCNP - A General Monte Carlo N-Particle Transport Code, Version 5*. Vol. 2. California: Los Alamos National Laboratory, 2003. Print.

26. Shleien, B., Lester A. Slaback, and Brain K. Birky. *Handbook of Health Physics and Radiological Health*. 3rd ed. Baltimore: Williams & Wilkins, 1998. Print.

27. "Density Of Copper." *Universe Today — Space and Astronomy News*. 1999. Web. <http://www.universetoday.com/82000/density-of-copper/>.

28. Ali, Fawaz. "On The Integration of Computational Fluid Dynamics (CFD) Simulations with Monte Carlo(MC) Radiation Transport Analysis." MSc Thesis. *UOIT-Library*. UOIT, Dec. 2009.

29. "Inverse Square Law." *HyperPhysics*. Georgia State University, 1997. Web. <http://hyperphysics.phy-astr.gsu.edu/hbase/forces/isq.html>.

30. Attix, Frank H. *Introduction to Radiological Physics and Radiation Dosimetry*. New York: Wiley, 1986. Print.

31. Hubbell, J. H., and S. M. Seltzer. "X-Ray Mass Attenuation Coefficients." *Tables of X-Ray Mass Attenuation Coefficients and Mass Energy-Absorption Coefficients from 1keV to 20MeV for Elements Z= 1 to 92 and 48 Additional Substances of Dosimetric Interest*. National Institute of Standards and Technology, 17 Sept. 2009. Web. <http://physics.nist.gov/PhysRefData/XrayMassCoef/tab3.html>.

32. "Annual Limit Intakes (ALI)." *Université D'Ottawa - University of Ottawa*. University of Ottawa. Web. <http://www.uottawa.ca/services/ehss/radali.htm>.

33. *VISED*. Computer software. Vers. 7M. July 2001.

34. *MCNP*. Computer software. Vers. 4A. Los Alamos.

35. Cadwallader, L. C., and S. A. Bruyere. "Stack Monitor Operating Experience Review." *Idaho National Laboratory*. Idaho National Laborator, May 2009. Web. <http://www.inl.gov/technicalpublications/Documents/4247159.pdf>.

36. Kupca, S., G. F. Lynch, R. J. Booth, J. M. Cuttler, J. E. Villagran, and V. K. Mohindra. "A High Sensitivity Noble Gas Stack Effluent Monitor for CANDU Power Reactors." *International Atomic Energy Agency*. Ontario Hydro, 9 June 1982. Web. <http://www.iaea.org/inis/collection/NCLCollectionStore/_Public/16/016/16016684.pdf>.

37. NRC: 10 CFR Part 20 - Appendix B - Radionuclide Table - Index of Radioisotopes." *NRC: Home Page*. Nuclear Regulatory Commission, 9 June 2011. Web. <http://www.nrc.gov/reading-rm/doc-collections/cfr/part020/appb/>.

38. Jones, Andrew Z. "The Compton Effect - an Introduction to the Compton Effect."*About.com.Physics*. The New York Times Company, 2011. Web. <http://physics.about.com/od/quantumphysics/a/comptoneffect.htm>.

39. *Stopping Power for Electrons and Positrons*. ICRU, Rep. 47. International Commission on Radiological Units and Measurments, October 1984. Print.

40. Kumar, Ashita. "An Experimental Study of the Relative Response of Plastic Scintillators to Photons and Beta Particles." Poster Presentation at UNENE Research and Development Workshop. Ontario, Mississauga. Nov. 2010. Poster Presentation.

41. Kumar, Ashita. "An Experimental Study of the Relative Response of Plastic Scintillators to Photons and Beta Particles." Health Physics Society – Midyear Meeting – Radiation Measurements. South Carolina, Charleston. Feb. 2011. Speech.